

Oxygen and silicon isotopic compositions of Archean silicified lava and cherts of the Onverwacht Group: Implication for seafloor hydrothermalism and the nature of recycled components in the source of granitoids

L.S. Kitoga^{a,b,*}, D. Zakharov^c, J. Marin-Carbonne^d, M. Boyet^a, J.-F. Moyen^a, T. Di Rocco^e, A. Pack^e, N. Olivier^a, G. Stevens^b

^a Laboratoire Magmas et Volcans, Université Clermont Auvergne, CNRS, IRD, OPGC, F-63000 Clermont-Ferrand, France

^b Department of Earth Sciences, University of Stellenbosch, Private Bag XI, Matieland 7602, South Africa

^c Department of Geological and Environmental Sciences, Western Michigan University, Kalamazoo 49008, USA

^d Institut des Sciences de la Terre, Université de Lausanne, 1015 Lausanne, Switzerland

^e Geowissenschaftliches Zentrum, Georg-August-Universität Göttingen, Göttingen, Germany

ARTICLE INFO

Editor: Dr. Don Porcelli

Keywords:

Chert
Silicified lava
Seafloor hydrothermalism
Palaeoarchean granitoids

ABSTRACT

Cherts are commonly used as proxies for Archean environmental conditions such as oceanic temperature. However, because cherts encompass a wide variety of silica-rich rocks, including post-depositional silicified of clastic sediments or chemical precipitates from seawater, reconstructions of the Archean environment based on their O and Si isotopic compositions remain controversial. In this study, we present triple O isotope analyses associated with SIMS O and Si isotope measurements of Palaeoarchean pervasively silicified lavas and clastic sediments, which have been less studied than the associated cherts within the Onverwacht Group (Barberton Greenstone Belt, South Africa). We also provide triple O isotopic compositions of seawater-precipitated cherts. The O and Si isotope composition of silicified clastic sediments and lavas is not considerably variable through the Onverwacht succession. These lithologies display relatively low $\delta^{18}\text{O}$ (11.3–14.9 ‰) and high $\Delta^{17}\text{O}$ values (−0.05 to −0.07 ‰) attributed to precipitation of silica from hydrothermal fluids at lower temperatures than 200 °C. Using these results, we reconstruct the approximate O isotope composition of the hydrothermal fluids. Water-rock interaction models suggest that this fluid composition is consistent with the existence of low $\delta^{18}\text{O}$ oceans, but the exact $\delta^{18}\text{O}$ value of the Palaeoarchean ocean remains elusive. Seawater-precipitated cherts show a mixture of hydrothermal and seawater-like triple O isotope signatures, confirming that cherts are not a straightforward proxy for constraining Archean seawater composition or temperature. The average $\delta^{30}\text{Si}$ value of the pervasively silicified lavas and clastic sediments is positive ($> +0.19$ ‰) and compositionally similar to published values of the seawater-precipitated cherts. This suggests comparable $\delta^{30}\text{Si}$ values between Archean hydrothermal fluids and seawater. A gradual increase of $\delta^{18}\text{O}$ values of silicified lavas and cherts from 10 to 13 ‰ to 15–20 ‰ observed along the Onverwacht succession is ascribed to local lithospheric cooling occurring between 3.47 Ga and 3.3 Ga, while Si isotope compositions remained mostly unchanged in the silica-rich rocks. As silicified lavas are likely part of materials that melted to generate Palaeoarchean granitoids, the evolutionary difference between O and Si isotopes may have characterised the silicified rocks that were recycled in different generations of granitoid sources. This may explain the variation in O isotopic compositions measured in different granitoid generations in the Barberton area.

1. Introduction

Interactions between Archean seawater and the submarine mafic rocks facilitated the generation of felsic and relatively buoyant

continental crusts (André et al., 2019; Martin et al., 2014; Tamblyn et al., 2023). On the modern Earth, infiltration of seawater and water-rock reactions driven by heat deep in the oceanic crust plays an important role in altering the composition of the oceanic crust and

* Corresponding author at: Laboratoire Magmas et Volcans, Université Clermont Auvergne, CNRS, IRD, OPGC, F-63000 Clermont-Ferrand, France
E-mail address: kitogastlevel@gmail.com (L.S. Kitoga).

<https://doi.org/10.1016/j.chemgeo.2024.122407>

Received 15 January 2024; Received in revised form 7 September 2024; Accepted 10 September 2024

Available online 12 September 2024

0009-2541/© 2024 The Authors. Published by Elsevier B.V. This is an open access article under the CC BY license (<http://creativecommons.org/licenses/by/4.0/>).

generating hydrothermal fluids (Alt et al., 2010; Alt and Bach, 2006; Elderfield et al., 1999; Shanks, 2001; Yu et al., 2023; Zakharov et al., 2021a). Hydrothermal fluids are compositionally different from seawater, and modulate the balance of many dissolved elements on geologically long timescales (Shanks, 2001). For the Archean Eon, greenstone belts likely represent the best archives of seawater-rock interactions. Archean greenstone belts are often composed of silicified lavas in which magmatic minerals were replaced by quartz through hydrothermal alteration of the Archean crust (e.g. Grosch and Slama, 2017; Hofmann et al., 2022). Some of these silicified lavas preserve their volcanic structures (e.g., pillows) and textures (e.g., spinifex and ocellar textures) while being completely replaced by a silica-rich cement (Hanor and Duschac, 1990; Paris et al., 1985). This process is termed silicification and is likely an intrinsic feature of seawater-rock interaction below the silica-rich Archean ocean.

In many greenstone belts, silicified lavas are intertwined with chert layers consisting of hydrothermally and/or diagenetically silicified clastic sediments and pure silica precipitated from seawater (Hofmann et al., 2013; Lanier and Lowe, 1982; Ledevin et al., 2019). These silica-rich lithologies not only reveal the chemistry of the Archean seawater (Holmden and Muehlenbachs, 1993; Jaffrés et al., 2007; Tatzel et al., 2022) and hydrothermal fluids (Bregman et al., 2016; Hofmann and Harris, 2008; Van Den Boorn et al., 2007), but can constrain also the composition of the altered crust that was reworked in the magma sources of Archean granitoids (André et al., 2019, 2022; Deng et al., 2019; Foley et al., 2003).

Recent measurements of O and Si isotope compositions in Archean granitoids have firmly supported the contribution of seafloor-derived silica to their source (André et al., 2019; Deng et al., 2019; Lei et al., 2023; Vezinet et al., 2018; Wang et al., 2022). However, interpretation of O and Si isotopic variations of Archean granitoids remains obstructed by the lack of data on the compositional evolution of recycled silicified lithologies. To determine pathways of recycled seafloor-derived silicified lithologies and decipher (or gain insight into) their potential relationship to granitoid signatures, a detailed investigation of variations in the O and Si isotope compositions of silicified lavas and cherts within a well-defined stratigraphic and petrographic framework from a single greenstone belt is needed.

Progressive O and Si isotope evolutionary trends recorded in global chert compilations have been interpreted as due to 1) secular cooling of oceans (Knauth and Lowe, 1978; Lowe and Byerly, 2020; Robert and Chaussidon, 2006), 2) to the evolution of seawater isotopic compositions (Herwartz et al., 2021; Jaffrés et al., 2007) or 3) to changes in diagenetic temperatures through time (Sengupta and Pack, 2018; Zakharov et al., 2021b). Importantly, several studies have highlighted the ambiguity in our understanding of the origin of Archean cherts as they could form from various processes including hydrothermal and diagenetic silicification of precursor sedimentary or volcanic material as well as direct chemical precipitation from seawater (Ledevin et al., 2014; Marin-Carbonne et al., 2011, 2012; Marin et al., 2010; Stefurak et al., 2015; van den Boorn et al., 2007, 2010). Moreover, in situ studies of O and Si isotopic variations in quartz cements have revealed the importance of diagenetic and later fluid circulation processes that can influence both O and Si isotope compositions of cherts (Cammack et al., 2018; Marin-Carbonne et al., 2012; Marin et al., 2010). Recent triple O isotope analyses (i.e. simultaneous measurements of $^{18}\text{O}/^{16}\text{O}$ and $^{17}\text{O}/^{16}\text{O}$ ratios) have also confirmed the importance of post-depositional processes such as diagenesis and regional metamorphism on O isotope compositions of cherts (Ibarra et al., 2022; Sengupta et al., 2020; Yanchilina et al., 2020; Zakharov et al., 2023). Due to the complexity of chert-forming processes, a quantitative determination of parental fluid O and Si isotope compositions is still challenging.

The first objective of this study was to constrain the isotope composition of Palaeoarchean hydrothermal fluids by characterizing Si ($^{28}\text{Si}/^{30}\text{Si}$) and O ($^{16}\text{O}/^{17}\text{O}/^{18}\text{O}$) isotopic compositions of 1) silicified lavas, 2) silicified clastic sediments and 3) seawater-precipitated cherts,

that represent different pathways of Archean aqueous silica, leading to a diversity of chert-forming mechanisms. The second objective was to place new constraints on the O isotope composition and temperature of the Palaeoarchean seawater using the diverse and well-characterised set of samples. Finally, the last objective was to provide a comprehensive suite of samples that could potentially represent the recycled material that contributed to the source of TTG magmas. This study was conducted on samples derived from the 3.5–3.3 Ga old Onverwacht Group of the Barberton Greenstone Belt, which includes portions of the Palaeoarchean submarine mafic crust (de Wit et al., 2011; Hofmann and Harris, 2008; Paris et al., 1985), and which is considered as analogous to the source of surrounding 3.5–3.1 Ga old granitoids (André et al., 2019, 2022; Deng et al., 2019; Lei et al., 2023).

2. Samples and methods

2.1. The Onverwacht Group

The Onverwacht Group is part of the 3.55–3.2 Ga Barberton Greenstone Belt located in the NE part of the Southern African Kaapvaal Craton (Fig. 1). It is one of the best-preserved records of an Archean seawater-altered crust, comprising alternating ultramafic to mafic lavas and silicified sediments that are commonly identified in the literature as “cherts” (Byerly et al., 1996; de Wit and Furnes, 2016; Hofmann and Harris, 2008). The Onverwacht Group includes six distinct geological formations that encompass in chronostratigraphic order the Sandspruit, Theespruit, Komati, Hoogenoeg, Kromberg and Mendon formations (Hofmann and Harris, 2008; Lowe and Byerly, 2007). Each of these formations is subdivided into different stratigraphic members and each member typically includes a mafic unit and a sedimentary or chert layer (Fig. 1b). Each volcanic eruption was followed by a period (up to >1 Ma) of volcanic quiescence during which cherts deposited and lava flow tops were silicified (Duschac and Hanor, 1987; Hofmann and Harris, 2008; Paris et al., 1985). The portion of the Onverwacht Group situated to the north of the Komati Fault (Fig. 1) was affected by a regional greenschist-facies metamorphic event (300–400 °C) (Alleon et al., 2021; Grosch, 2018; Tice et al., 2004; Xie et al., 1997).

The chert units of the Onverwacht Group include pervasively silicified detrital sediments and pure silica precipitates that are all dominated by more than 90 vol% of microquartz (Hofmann et al., 2013; Ledevin et al., 2019; Rouchon and Orberger, 2008). These pervasively silicified clastic sediments generally preserve sedimentary features including normal grading of clastic components at the outcrop scale (Duschac and Hanor, 1987; Lanier and Lowe, 1982; Ledevin et al., 2014; Paris et al., 1985; Rouchon and Orberger, 2008). They are by far the dominant member of the chert family, generally appearing in the field as black, grey or black-and-white banded chert layers (Hofmann et al., 2013; Lanier and Lowe, 1982; Lowe et al., 2020; Lowe and Byerly, 1986; Fig. 2a). Pure chemical cherts are quite rare in the Onverwacht Group and may include the detritus-free banded chert layers of the Buck Reef Chert Unit located at the bottom of Kromberg Formation and similar rocks from the Mendon formation (Ledevin et al., 2019; Lowe and Byerly, 2020; Stefurak et al., 2015). The $\delta^{18}\text{O}$ value of cherts from the Onverwacht Group gradually increases gradually from ~11–13 ‰ at the base and the Buck Reef Chert displays some of the highest $\delta^{18}\text{O}$ values of this stratigraphic succession (up to 22 ‰, see at 7 km) (Fig. 3a-b) (Abraham et al., 2011; de Wit and Furnes, 2016; Knauth and Lowe, 1978, 2003; Lowe and Byerly, 2020). In contrast, the $\delta^{30}\text{Si}$ of these cherts does not show a systematic variation over the stratigraphic column (Fig. 3c).

The topmost lava units of the Onverwacht Group evolve downwards from pervasively silicified lava that recorded intense interactions with Si-rich hydrothermal fluids, to non-silicified lava (Abraham et al., 2011; Hofmann and Harris, 2008; Paris et al., 1985). The silicified lavas feature original magmatic structures (e.g. pillows – see Fig. 2b – and spinifex or ocellar textures) or structures that are typical of

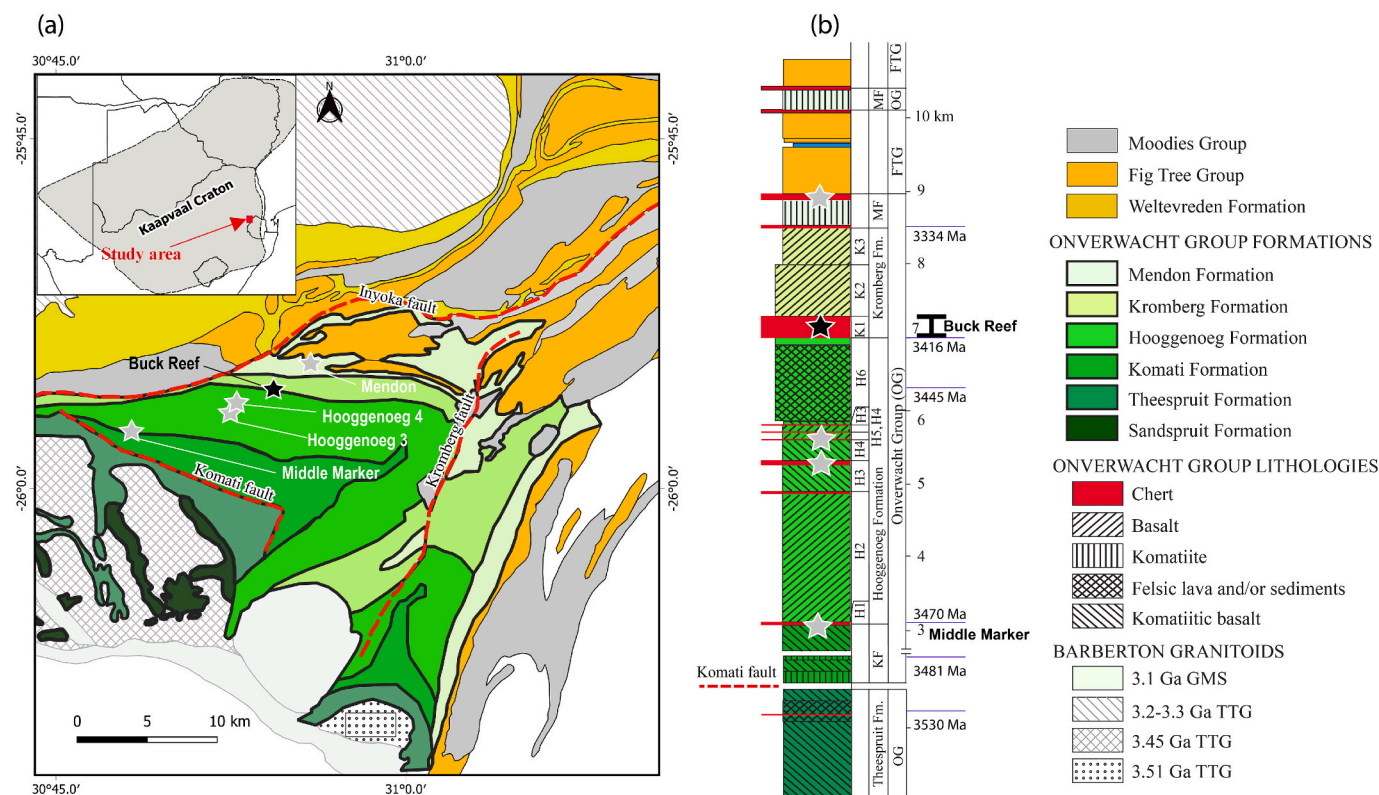


Fig. 1. Geological map (a) and lithostratigraphy (b) of the Barberton Greenstone Belt. The geological map and lithostratigraphic section, together with existing geochronological constrains were modified from Byerly et al. (2019) and Hofmann (2005). Black stars are indicative of the Buck Reef Chert locality which represent seawater-precipitated cherts while the grey stars are representative of silicified clastic sediment and lavas from the Middle Marker, Hooggenoeg 3, Hooggenoeg 4 and Mendon 1 stratigraphic members.

hydrothermal environments (e.g. brecciated textures) (Hofmann and Harris, 2008; Lowe and Byerly, 1986; Paris et al., 1985). Pervasively silicified lavas consist of >80 vol% microscopic quartz (hereinafter, microquartz) and minor assemblages of phyllosilicate phases (i.e. chlorite and muscovite), Fe—Ti oxides, carbonates and sulphides (Hofmann and Harris, 2008). Silicified lavas and cherts are all extremely fine-grained, such that separation of minor and accessory phases from quartz for selective isotopic analysis is not possible. Previously collected bulk-rock isotopic compositions of O and Si in partially and pervasively silicified lavas from the Onverwacht Group ($\delta^{18}\text{O}$ of 10.5–15.6 ‰ and $\delta^{30}\text{Si}$ of -0.64 to 0.74 ‰) are shown in Fig. 3 (Abraham et al., 2011; de Wit and Furnes, 2016; Hofmann and Harris, 2008).

2.2. Sample description

In this study, we analysed three different groups of samples: 1) silicified lava, 2) silicified clastic sediments and 3) seawater-precipitated cherts. The first sample group comprises six pervasively silicified lava samples collected respectively from the Middle Marker (number of samples or $n = 1$; SK-MM11), Hooggenoeg 3 ($n = 2$; SK-HO09 and SK-HO12) and Mendon 1 ($n = 3$; SK-ME17, SK-ME18 and SK-ME20) members of the Onverwacht Group (Fig. 1). These samples derived from variable depths below chert layers (1 to 40 m), but they all contain more than 90 vol% of microquartz testifying their pervasive silicification. The second group of samples includes seven cherts representing pervasively silicified clastic sediments derived from the Middle Marker ($n = 4$; MM07–11, MM07–10, MM24 and MMJLog53), Hooggenoeg 3 ($n = 1$; SK-HO05) and Hooggenoeg 4 ($n = 2$; SK-HO25 and SK-HO26) stratigraphic members. Finally, the third sample group is constituted by nine seawater-precipitated chert samples that originated from the Buck Reef Chert (Buck4A plus eight BBDP samples obtained from the

BARB4 ICDP drill core) located at the base of the Kromberg Formation (Ledevin et al., 2019; Lowe et al., 2020).

Petrographic descriptions allow identifying four different types of quartz in both the silicified lavas and silicified clastic sediment samples that we analysed by SIMS (Fig. 4). The first and most dominant type is a microquartz made of micro-sized (<30 μm) crystals that make up more than 90 % of the rock (Fig. 4a) with minor phases of phyllosilicates (chlorite and muscovite), carbonates, oxides, sulphides and phosphates. The second type of quartz corresponds to veins (Fig. 4b-c) made of coarser quartz crystals (<70 μm), with additional minor assemblages of Fe oxide and carbonate phases. The third quartz type corresponds to megaquartz (Fig. 4c). This cement of coarse-grained quartz crystals (>150 μm) occurs as void-filling aggregates. Finally, the fourth type of quartz is represented by inclusions within carbonate phases (i.e. calcite in SK-MM11 and ankerite in SK-ME18). These quartz inclusions are made of polycrystalline assemblages to monocrystalline euhedral quartz (Fig. 4d).

2.3. O and Si isotope analyses

In addition to published datasets on O and Si isotope variations in cherts and silicified lavas from the Onverwacht Group (Fig. 3) (Abraham et al., 2011; de Wit and Furnes, 2016; Geilert et al., 2014; Hayles et al., 2019; Hofmann and Harris, 2008; Knauth and Lowe, 1978, 2003; Marin-Carbonne et al., 2011; Stefurak et al., 2015; Zakharov et al., 2021), here we analysed the triple O isotope composition of all the samples described in the previous section excepted one silicified lava (SK-ME18). We also conducted SIMS analyses in five selected samples including one silicified clastic sediment (SK-HO25) and four pervasively silicified lavas (SK-MM11, SK-HO09, SK-ME17 and SK-ME18) that are representative of three different geological formations of the Barberton Greenstone Belt,

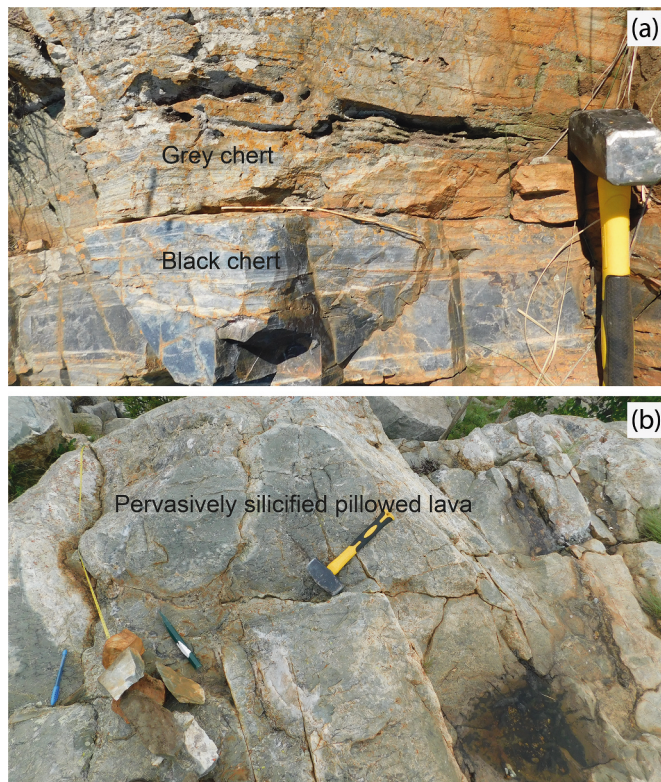


Fig. 2. An illustration of field occurrence of pervasively silicified cherts (a) and pillowed lava (b). Note that the pervasively silicified lavas crop out as greenish lithologies with common preservation of their original volcanic structures (e.g. pillows), whereas cherts occur as grey and black layers locally preserving some sedimentary features.

namely the Komati, Hooggenoeg and Mendon formations.

2.3.1. Notations

The delta notation of stable isotope ratios in a sample quantifies their relative difference from ratios of the same isotopes in a reference material (i.e. V-SMOW for O and NBS-28 for Si isotopes) and is expressed in the following equations:

$$\delta^X\text{O} = 1000 \times \left[\frac{(^X\text{O}/^{16}\text{O})_{\text{sample}}}{(^X\text{O}/^{16}\text{O})_{\text{VSMOW}}} - 1 \right]$$

with X representing either 18 or 17;

$$\delta^{30}\text{Si} = 1000 \times \left[\frac{(^{30}\text{Si}/^{28}\text{Si})_{\text{sample}}}{(^{30}\text{Si}/^{28}\text{Si})_{\text{NBS-28}}} - 1 \right]$$

The definition of $\Delta^{17}\text{O}$ is given by:

$$\Delta^{17}\text{O} = \delta^{17}\text{O} - 0.528 \times \delta^{18}\text{O},$$

where $\delta^{17}\text{O}$ and $\delta^{18}\text{O}$ are linearized delta expressions:

$$\delta^{18(17)}\text{O} = 1000 \times \ln(\delta^{18(17)}\text{O} / 1000 + 1).$$

2.3.2. Secondary ion mass spectrometry (SIMS)

Analyses of O and Si isotopic compositions of quartz by secondary ion mass spectrometry were carried out within the SwissSIMS laboratory at the University of Lausanne (UNIL), using the CAMECA 1280 HR secondary ion mass spectrometer. Selected zones (3 × 4 cm) of thin sections were imaged under a polarising microscope, isolated by a high precision diamond wire-saw and pressed into indium mounts together with the UNIL-Q1 reference quartz (Seitz et al., 2017). The surface of indium mounts did not exceed 5 μm of elevation difference, as determined with a Bruker GTA-K white light interferometer. After carbon coating and imaging by scanning electron microscopy at the Laboratoire Magmas et Volcans, University Clermont Auvergne, the carbon coat was removed by polishing, and the surface of each mount was cleaned with pure ethanol and distilled water, then dried in an oven and coated with a ~ 20 nm-thick gold layer. The samples were measured during two O

isotope analyses sessions and two Si isotope session.

A 10 kV, the primary beam of Cs⁺ ions was tuned at 1.3 nA for O isotopes and ~ 2 nA for Si isotopes and focused to a diameter of 15 μm. A current of -10 kV was applied using an electron gun to compensate the charge following the routine SIMS procedure. The mass resolving power was set at 2400 using an entrance slit of 122 μm and multicollection exit slit 1. Each O isotope analysis lasted ~3 min that included 30 s of pre-sputtering, followed by automatic signal optimization by centring the secondary beam, and 20 cycles of 5 s of secondary ion collection. For Si isotope measurements, analysis time was 3.5 min and included 1 min of pre-sputtering of the targeted surface, automatic centring of the secondary ions and 25 cycles of 5 s of measurements. ¹⁶O⁻, ¹⁸O⁻, ²⁸Si⁻ and ³⁰Si⁻ were detected in multicollection mode using Faraday cups; L2 trolley for ¹⁶O⁻ and ²⁸Si⁻ (using a 10¹⁰ Ω resistor for ¹⁶O⁻ and 10¹¹ Ω resistor for ²⁸Si⁻) and H1 trolley for ¹⁸O⁻ and ³⁰Si⁻ (both using a 10¹¹ Ω resistor).

Repeated analyses of UNIL-Q1 reference quartz allowed correcting for instrumental mass fractionation and provided an external error (2 S.D.) of 0.2–0.6 ‰ for δ¹⁸O and 0.5–0.7 ‰ for δ³⁰Si values depending on the analytical sessions.

2.3.3. Triple O isotopic analyses

Triple O isotopic analyses of 1–2 mg of silica chips isolated from each sample were analysed at the Geoscience Centre of Göttingen University, following the method previously described by Pack et al. (2016). The analysis of O isotopes was conducted by laser fluorination-assisted mass spectrometry. The O₂ gas was liberated from silica by a reaction with BrF₅ and purified from potential contaminants via a series of cryogenic traps. The purified O₂ was then absorbed onto 5 Å molecular sieves, and subsequently passed through a gas chromatograph via a He gas flow at 10 mL/min. After the evacuation of He carrier gas, the resultant O₂ was measured in dual inlet mode using a MAT253 instrument. The San Carlos olivine standard (Δ¹⁷O = - 0.052 ‰) was used for calibrations of δ¹⁷O on V-SMOW scale. The analytical reproducibility (i.e. the 2 S.D. value obtained from repeated analyses of San Carlos olivine) was better than ±0.6 ‰ for δ¹⁸O and ± 0.02 ‰ for Δ¹⁷O. We also used the laser fluorination technique to analyse the δ¹⁸O values of duplicates of the samples at the University of Lausanne. During these analyses, repeated measurements of the δ¹⁸O value of LS1 quartz standard (δ¹⁸O = 18.1 ‰) provided an external reproducibility (2 S.D.) of 0.2 ‰.

2.4. Modelling komatiite-seawater interaction and triple O isotope composition of resulting fluids

To model the triple O isotope and chemical composition of aqueous fluids produced by equilibrium reaction between a komatiite and seawater, we used a modelling software that computes heterogeneous aqueous-mineral equilibria. The CHIM-XPT program (Reed et al., 2010) was used to compute dissolved aqueous species and equilibrium minerals as a function of changing bulk composition, representing a series of titration steps of komatiite into 1 L of solution. The equilibrium speciation of aqueous species and mineral saturation indices (i.e., logQ/K's) are computed by the CHIM-XPT software for a series of incremental titration steps with intermittent calculation of equilibrium speciation by minimization of the Gibbs Free Energy of the system. The thermodynamic and related data for calculation of aqueous and mineral species are given in the description of the modelling software, particularly in the SOLTHERM database used by the CHIM-XPT software (Reed et al., 2010). CHIM-XPT uses Newton-Raphson method to solve a system of simultaneous mass-balance and mass-action equations and compute equilibrium activities of the aqueous and mineral species. In this study, we simulated an Archean seawater-komatiite reaction at 200 °C and 150 bars.

The initial compositions of reacting seawater and komatiite were set in the beginning of the calculation and the water/rock ratio is defined as a function of titrated komatiite. The initial seawater composition was

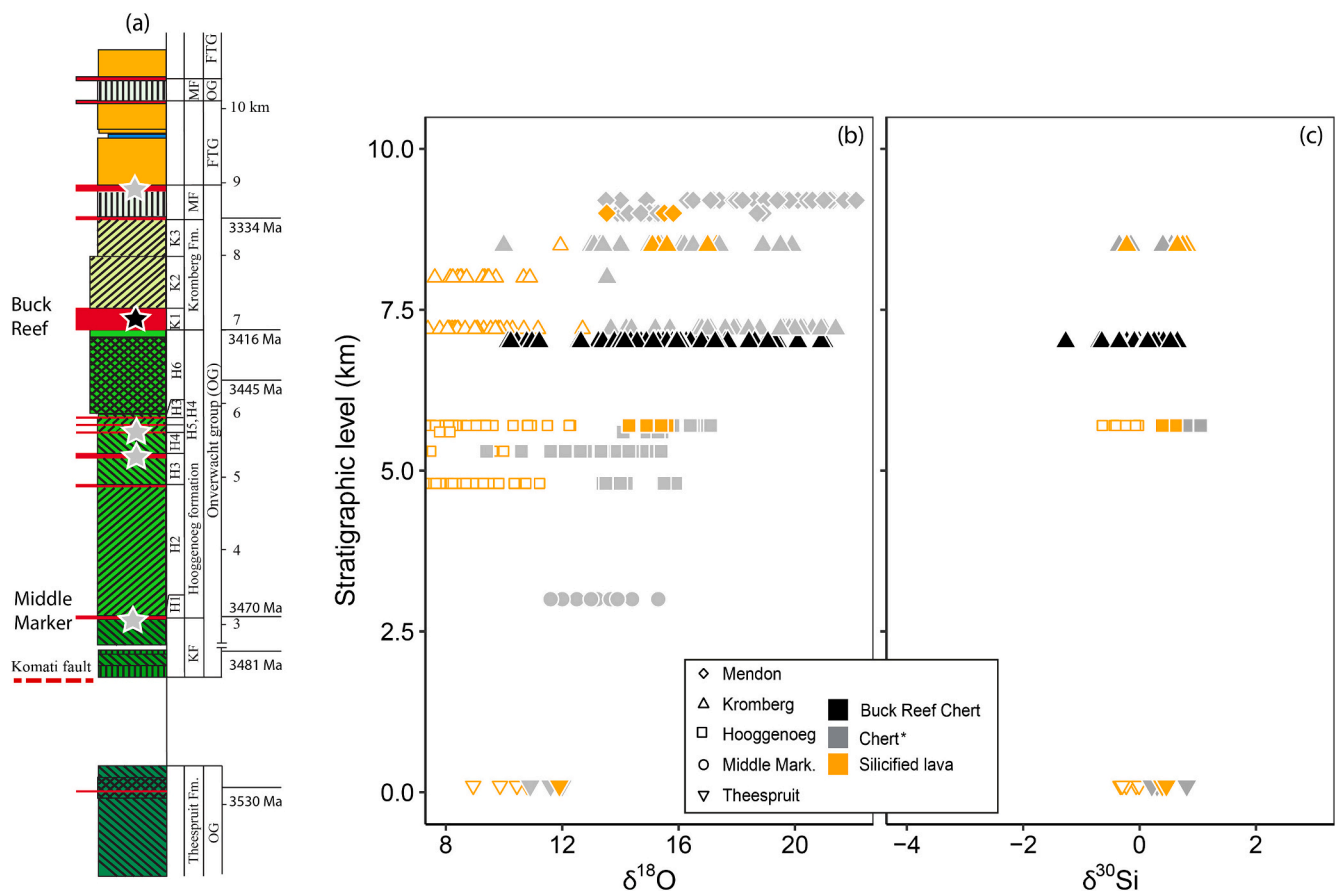


Fig. 3. Stratigraphic succession of the Onverwacht Group (a) and a compilation of previously analysed oxygen (b) and silicon (c) isotopic compositions in cherts (including silicified clastic sediments and seawater-precipitated cherts) and silicified lava from the Onverwacht Group plotted against stratigraphic positions. In filled symbols are silicified lavas and cherts with and SiO_2 content exceeding 60 wt%, while open symbols are lavas with a lower SiO_2 inferior to 60 wt%. Only bulk-rock data are shown on this figure, and they were compiled from the following works: Abraham et al. (2011), de Wit and Furnes (2016), Geilert et al. (2014), Hofmann and Harris (2008), Knauth and Lowe (1978, 2003), Lowe and Byerly (2020). The seawater-precipitated cherts of the Buck Reef Chert are plotted in black, while other cherts are in grey and silicified lava are in orange. The star (*) on cherts in the legend indicates that they may comprise pervasively silicified clastic sediments and seawater-precipitated cherts that were not clearly distinguished in the literature.

taken as a close analogue to the modern seawater (Bernier and Bernier, 1996), with the only modification that H_4SiO_4 concentration was fixed by an equilibrium with amorphous silica at 25 °C and the sulfate concentration is set extremely low. Such seawater (see **Supplementary File A**) represents a simplified composition of reduced Archean seawater that was probably saturated in silica, as attested by the abundance of cherts in Archean greenstone belts. The model is not aimed to fully reproduce the details of chemical speciation of the Archean seawater as it remains poorly constrained. However, this simple aqueous-mineral equilibrium reaction modelling is used to constrain the mass balance of the O isotope exchange trajectory between fluids and silicate rocks, where O is a major element, and silicate minerals and H_2O are major phases. The major elemental composition of seawater used in the calculations was set to (in mmol/kg): Cl = 594, Na = 457, Ca = 10.2, Mg = 53.6, K = 10.0, H_4SiO_4 = 15.7. The molality of Fe^{2+} (total dissolved species) and HCO_3^- ions were set to 0.2 and 389 $\mu\text{mol/kg}$, respectively. The composition of titrated komatiitic rock was taken as follows: Na_2O = 0.1 wt%, K_2O = 0.01 wt%, MgO = 28.1 wt%, FeO = 12.8 wt%, Al_2O_3 = 4.4, SiO_2 = 47.3 wt%.

To track the O isotope budget of the reaction, we assigned an isotope composition of mantle-derived lava to the fresh unaltered komatiite: $\delta^{18}\text{O}$ = 5.7 ‰ and a $\Delta^{17}\text{O}$ = -0.06 ‰ (Pack et al., 2016). Two end-member seawater compositions were used in the calculation. In the first case, seawater was taken with $\delta^{18}\text{O}$ and $\Delta^{17}\text{O}$ values of 0 ‰ like modern seawater. In the second case, we used a seawater with $\delta^{18}\text{O}$ of

-10 ‰ and a $\Delta^{17}\text{O}$ of +0.01 ‰ to reflect a potential low- $\delta^{18}\text{O}$ seawater proposed for the Archean Earth (Bindeman and O'Neil, 2022; Jaffrés et al., 2007; Sengupta and Pack, 2018; Zakharov et al., 2021). The triple O isotope composition of modelled equilibrium fluids was calculated using the mass-balance of O moles in the system distributed between equilibrium minerals and H_2O , taking into account mineral-water equilibrium fractionation factors derived from Wostbrock and Sharp (2021), Yapp (1990) and Zheng (1993). The $^{17}\text{O}/^{16}\text{O}$ fractionation factor is derived from the relationship $^{17/16}\alpha = ^{18/16}\alpha^\theta$. The theta value (θ) of 0.527 is adapted to calculate the ^{17}O fractionation factor based on the relationship for quartz-water equilibrium fractionation at 200 °C (Wostbrock and Sharp, 2021). Further details on the setup of the komatiite-seawater model can be found in **Supplementary File A**.

3. Results

3.1. Measured O and Si isotopic compositions

The triple O isotopic compositions measured in Göttingen and the $\delta^{18}\text{O}$ values measured in duplicate samples at UNIL by laser-fluorination are available in Table 1. In addition, the O and Si isotopic compositions acquired by SIMS are summarized in Table 2 (the detailed dataset is provided in Supplementary File B). The $\delta^{18}\text{O}$ values measured by SIMS and laser fluorination (both at Göttingen and Lausanne) are similar within the range of analytical error of the respective methods. SIMS

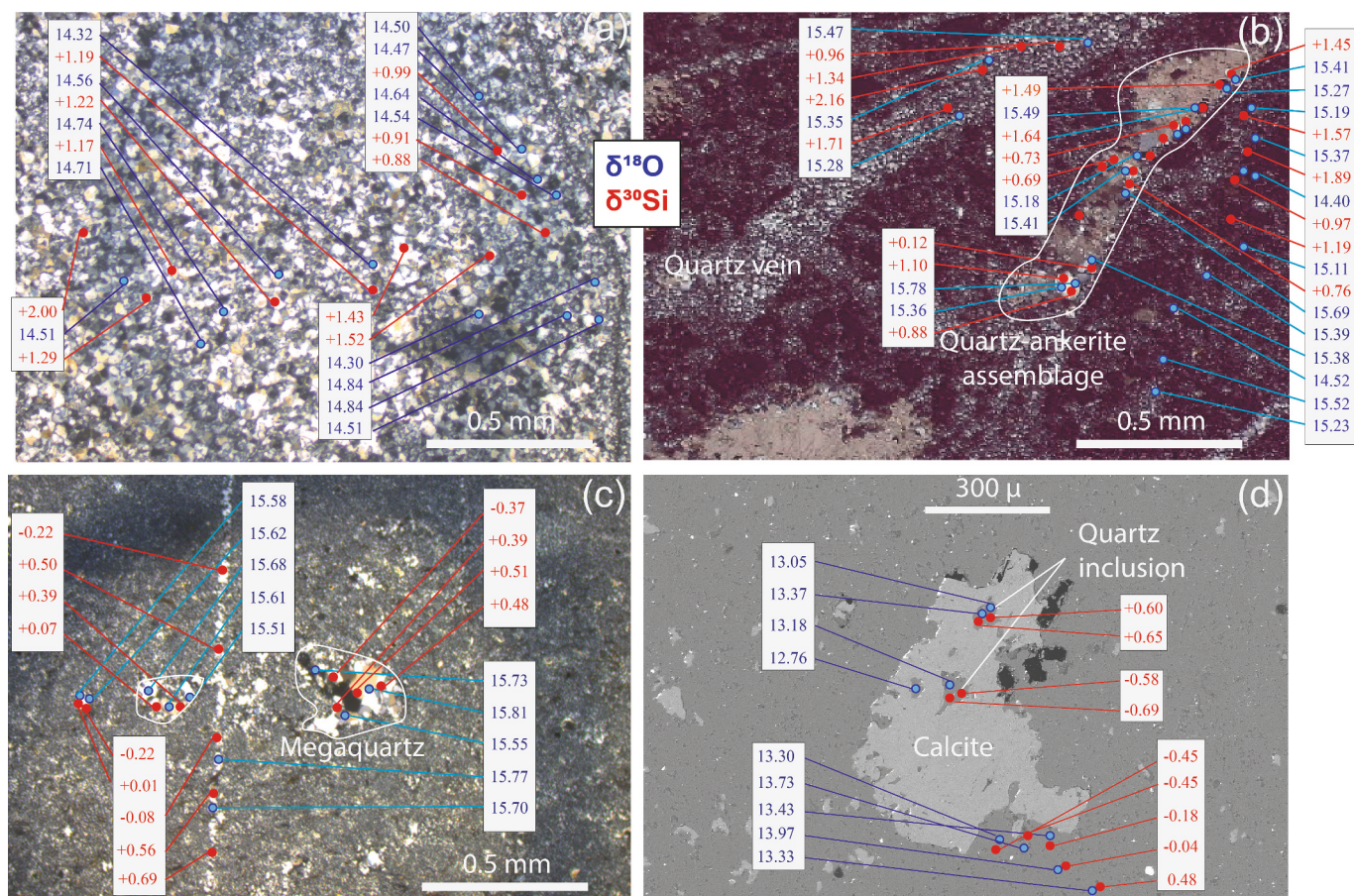


Fig. 4. Selected petrographic features of the analysed quartz cements with the SIMS $\delta^{18}\text{O}$ (in blue) and $\delta^{30}\text{Si}$ values (in red) of analysed spots. (a): microquartz cement of the silicified pillowed lava SK-HO09. (b): microquartz, veins and inclusions in carbonate in sample SK-ME18. (c): an aggregate of granoblastic quartz individualised in the fine-grained matrix and in a relatively thin quartz vein of sample SK-HO25. (d): a back-scattered electron image of sample SK-MM11 showing analysed quartz inclusions in calcite. (For interpretation of the references to colour in this figure legend, the reader is referred to the web version of this article.)

analyses enabled the independent measurement of $\delta^{18}\text{O}$ and $\delta^{30}\text{Si}$ of four types of quartz identified in our samples, i.e. microquartz, quartz veins, megaquartz and quartz inclusions in carbonates (Fig. 4). These four different quartz types display similar $\delta^{18}\text{O}$ and $\delta^{30}\text{Si}$ values in samples collected from the same geological formations (i.e. Komati, Hooggenoeg and Mendon formations) (Fig. 5). Because the only silicified clastic sediments analysed by SIMS (SK-HO25) is indistinguishable (within error) from the silicified lava of the Hooggenoeg Formation (SK-HO09) in terms of Si and O isotope compositions, their compositions are combined in Fig. 5.

The bulk $\delta^{18}\text{O}$ measured in pervasively silicified lavas ranges between 12.3 and 14.9 ‰, while pervasively silicified sediments have $\delta^{18}\text{O}$ values ranging between 11.3 and 14.2 ‰. These values are lower than the bulk $\delta^{18}\text{O}$ values of seawater-precipitated cherts from the Buck Reef Unit that we analysed, extending between 16.4 and 20.3 ‰ (Figs. 5 and 6). Average $\delta^{18}\text{O}$ values analysed by SIMS in the silicified lava and clastic sediment samples range between 13.5 and 15.5 ‰, and are restricted at the lower end of SIMS-determined microscale $\delta^{18}\text{O}$ ranges in seawater-precipitated cherts from the Buck Reef Unit and from the Mendon Formation (Figs. 5) (Marin-Carbonne et al., 2011; Stefurak et al., 2015). Individual samples depict narrow $\delta^{18}\text{O}$ variations (< 2 ‰) comprising the different quartz cements that were analysed (i.e. microquartz, quartz veins, megaquartz and quartz inclusions in carbonates). Although quartz inclusions in carbonate phases typically extend to slightly lower $\delta^{18}\text{O}$ values in SK-MM11 (13.1 ± 0.4 ‰) and SK-ME18 (14.9 ± 1.3 ‰) silicified lava samples (Table 2 and Fig. 4), quartz inclusion in carbonate remains globally indistinguishable from the other types of quartz within the analytic error (2 S.D. = 0.6 ‰). Both SIMS and

laser fluorination data display a similar pattern of increasing $\delta^{18}\text{O}$ values (Fig. 5) that is overall consistent with stratigraphic increase of $\delta^{18}\text{O}$ values in cherts upwards through the Onverwacht succession (Fig. 3). The $\Delta^{17}\text{O}$ of pervasively silicified lava and silicified clastic sediment samples range between -0.07 to and -0.05 ‰, covering a narrower range with higher values than seawater-precipitated cherts from the Buck Reef Unit (-0.12 to to -0.07 ‰) (Fig. 6).

The SIMS-determined $\delta^{30}\text{Si}$ values of analysed spots vary between -2.1 and +2.3 ‰ with no textural control on this variable within our error limits (2 S.D. = 0.5–0.7 ‰) (Fig. 5). Average values of $\delta^{30}\text{Si}$ per sample are generally positive, ranging between +0.19 and +1.24, consistently with bulk-rock analyses of Si isotopes in the silicified lavas and silicified clastic sediments from the Onverwacht Group (Abraham et al., 2011; Geilert et al., 2014). Unlike $\delta^{18}\text{O}$, there is no general stratigraphic trend of $\delta^{30}\text{Si}$ variation along the Onverwacht Group in our dataset. This is consistent with the absence of a positive correlation between $\delta^{18}\text{O}$ and $\delta^{30}\text{Si}$ values in pervasively silicified lavas and clastic sediments throughout the Onverwacht stratigraphy contrary to previous observation (Abraham et al., 2011). The positive correlation between $\delta^{18}\text{O}$ and $\delta^{30}\text{Si}$ observed in Abraham et al. (2011) is due to a combination of non-silicified lava, silicified lava and chert samples with variable SiO_2 content (39.7 to 100 wt%) (see Figure in Supplementary File C).

3.2. Modelling results

In our model of seawater-komatiite interactions at 200 °C, secondary minerals equilibrated include amphiboles (e.g. tremolite and actinolite), chlorites (e.g. daphnite, clinocllore) and serpentines (e.g. chrysotile)

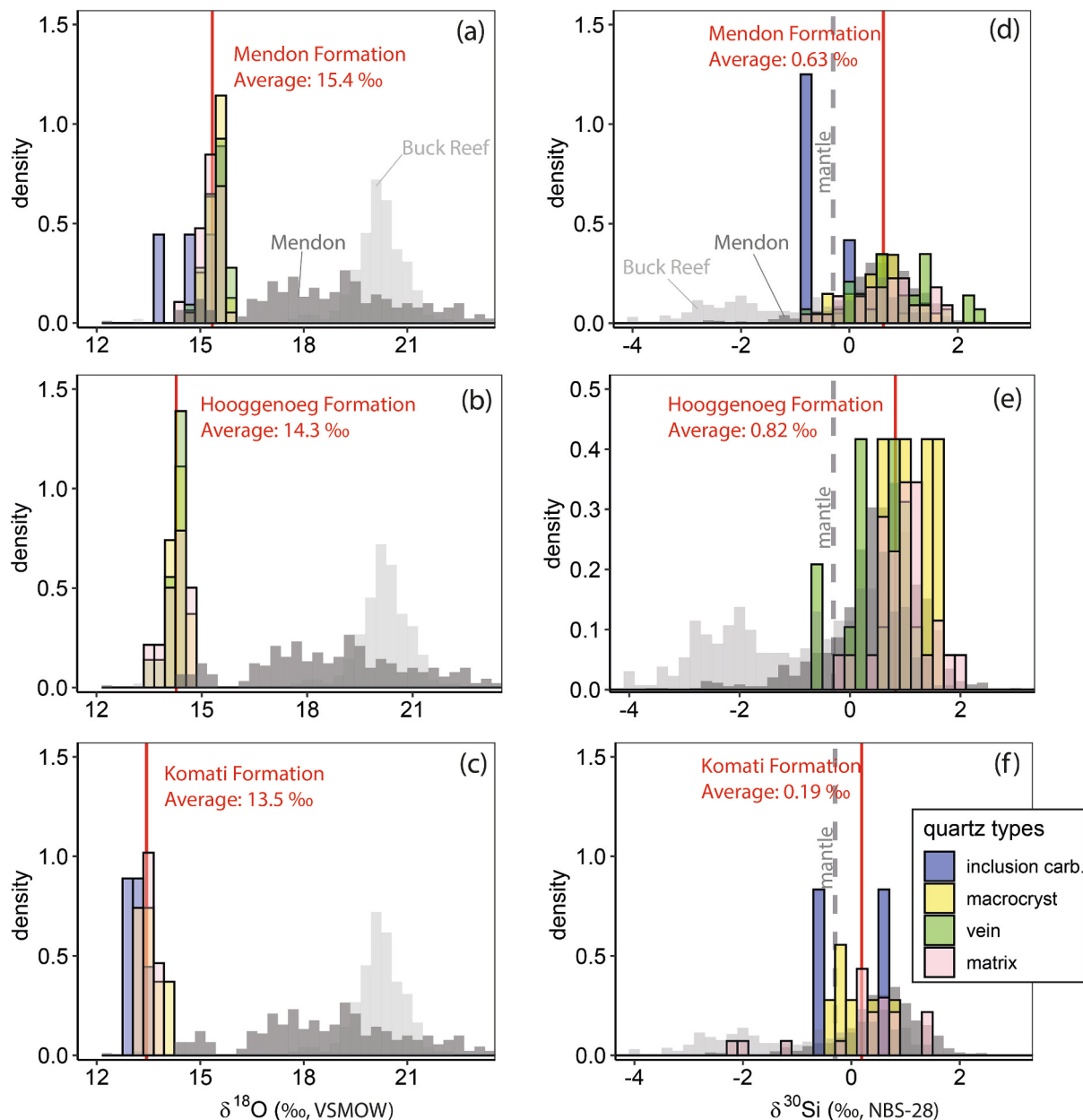


Fig. 5. (a) to (f) Histograms presenting the SIMS-determined variations of O and Si isotopic compositions classified by microquartz matrix, quartz vein, megaquartz and carbonate-included quartz analyses within the Komati, Hooggenoeg and Mendon samples. The compositions of silicified lava and clastic sediments analysed in this study are compared with isotopic variations in seawater-precipitated Buck Reef and Mendon cherts published by [Marin-Carbonne et al. \(2011\)](#) and [Stefurak et al. \(2015\)](#).

that precipitated in equilibrium with a residual fluid virtually representing the silicifying hydrothermal fluid (Fig. 7a). The triple O isotope composition of seawater inputted into the model influences considerably the isotopic composition of modelled hydrothermal fluid. When a seawater characterised by a $\delta^{18}\text{O}$ of -10 ‰ and a $\Delta^{17}\text{O}$ of 0.01 ‰ is considered in the model, the $\delta^{18}\text{O}$ of computed hydrothermal fluid remains negative, ranging between -10 and -0.1 ‰ across different water/rock ratios (10^5 to 0.3) (Fig. 7b). If the triple O composition of modern seawater is inputted ($\delta^{18}\text{O} = 0$ ‰ and $\Delta^{17}\text{O} = 0$ ‰), the computed $\delta^{18}\text{O}$ of computed hydrothermal fluid increases from 0 to 2 ‰ over the considered range of water/rock ratio (Fig. 6b). Notably, the $\Delta^{17}\text{O}$ of the modelled hydrothermal fluids is generally negative, ranging from $+0.01$ to -0.04 , and shows insignificant variation between the two different seawater compositions considered in the model (Fig. 6c).

4. Discussion

The silicified lavas, silicified clastic sediments and seawater-precipitated cherts investigated in this study are among the best records of Palaeoarchean seawater-derived hydrothermal fluids that circulated during their formation near the seafloor between 3.47 and 3.3 Ga ago (Fig. 1) ([Abraham et al., 2011](#); [de Wit and Furnes, 2016](#); [Marin-Carbonne et al., 2011, 2013](#); [Van Den Boorn et al., 2007](#)). Notably, a distinct difference between hydrothermally silicified lavas or clastic sediments and seawater-precipitated cherts is identified in O isotope composition but not in Si isotope composition (Figs. 5 and 7). These isotopic compositions represent important aspects in understanding the composition and temperature of the Palaeoarchean hydrothermal fluids and seawater from which silica precipitated. Nevertheless, it is important to consider the potential influence of late-

Table 1
Measured triple O isotopic compositions.

Sample	Unit	Lithofacies	Meters below sediment	$\delta^{18}\text{O}$ (‰)_UNIL	$\delta^{18}\text{O}$ (‰)	$\delta^{17}\text{O}$ (‰)	$\delta^{18}\text{O}$ (‰)	$\delta^{17}\text{O}$ (‰)	$\Delta^{17}\text{O}$ (‰)
SK-ME17	Mendon 1	Silicified lava	9 m	14.9	14.8	7.7	14.7	7.7	-0.06
SK-ME20	Mendon 1	Silicified lava	14 m	15.1	14.2	7.4	14.1	7.4	-0.06
SK-HO09	Hooggenoeg 3	Silicified pillow	15 m	14.0	12.7	6.6	12.6	6.6	-0.07
SK-HO12	Hooggenoeg 3	Silicified pillow	35 m	13.8	12.8	6.7	12.8	6.7	-0.06
SK-MM11	Middle Marker	Silicified pillow	1 m	13.1	12.3	6.4	12.2	6.4	-0.05
SK-HO25	Hooggenoeg 4	silicified sediment		14.2	13.8	7.2	13.7	7.1	-0.06
SK-HO26	Hooggenoeg 4	silicified sediment		13.8	13.2	6.9	13.2	6.9	-0.06
SK-HO05	Hooggenoeg 3	silicified sediment		12.4	11.7	6.1	11.7	6.1	-0.06
MM07-11	Middle Marker	silicified sediment		12.1	11.3	5.9	11.2	5.9	-0.05
MM07-10	Middle Marker	silicified sediment		12.7	11.9	6.2	11.9	6.2	-0.07
MM24	Middle Marker	silicified sediment		12.8	12.5	6.5	12.4	6.5	-0.07
MMJLog53	Middle Marker	silicified sediment			13.0	6.7	12.9	6.7	-0.07
Buck4A	Buck Reef	seawater-prec. Chert			16.4	8.5	16.3	8.5	-0.07
BBDP12724	Buck Reef	seawater-prec. Chert			19.9	10.3	19.7	10.3	-0.09
BBDP11265	Buck Reef	seawater-prec. Chert			20.3	10.6	20.1	10.5	-0.10
BBDP8545	Buck Reef	seawater-prec. Chert			19.9	10.4	19.7	10.3	-0.09
BBDP13784	Buck Reef	seawater-prec. Chert			19.5	10.1	19.3	10.1	-0.11
BBDP8545	Buck Reef	seawater-prec. Chert			19.9	10.4	19.7	10.3	-0.10
BBDP8545	Buck Reef	seawater-prec. Chert			19.3	10.0	19.1	10.0	-0.10
BBDP13784	Buck Reef	seawater-prec. Chert			19.3	10.0	19.1	10.0	-0.10
BBDP13784	Buck Reef	seawater-prec. Chert			17.7	9.2	17.6	9.2	-0.10

Table 2
Summary of SIMS-determined oxygen and silicon isotopic compositions.

Sample	Formation	Lithofacies	quartz type	OXYGEN ISOTOPE DATA			SILICON ISOTOPE DATA		
				#spots	$\delta^{18}\text{O}$ (‰)	2 S.D.	#spots	$\delta^{30}\text{Si}$ (‰)	2 S.D.
SK-ME17	Mendon	Silicified lava	matrix	16	15.54	0.37	13	0.65	0.72
			Granoblast	15	15.51	0.47	16	0.07	0.74
			vein	9	15.71	0.20	9	0.13	0.91
SK-ME18	Mendon	Silicified lava	matrix	26	15.13	0.59	24	0.75	1.63
			Granoblast	19	15.41	0.45	20	0.75	0.89
			vein	15	15.26	0.49	15	1.38	1.02
SK-HO25	Hooggenoeg	Black chert	Incl. Ank.	7	14.90	1.25	4	-0.57	0.89
			matrix	18	14.10	0.77	17	0.81	1.03
			Granoblast	6	14.34	0.27	4	1.12	0.92
SK-HO09	Hooggenoeg	Silicified lava	vein	16	14.24	0.47	16	0.49	1.14
			matrix	13	14.52	0.38	11	1.24	0.65
			matrix	25	13.49	0.39	23	0.25	1.81
SK-MM11	Komati	Silicified lava	Granoblast	6	13.55	0.52	6	0.09	0.95
			Incl. Carb.	5	13.09	0.44	4	-0.01	1.45

stage processes such as regional metamorphism that affected the entire Barberton Greenstone Belt around 3.2 Ga ago (Grosch, 2018; Tice et al., 2004; Xie et al., 1997). This metamorphism could potentially modify the isotopic composition of the studied rocks (Knauth and Lowe, 2003). We therefore explore first the potential effects of regional metamorphism on the measured isotopic compositions. Subsequently, we discuss implications for the O and Si isotopic composition of Paleoproterozoic near-seafloor hydrothermal fluids, and evaluate the influence of hydrothermal fluid circulation on the composition of seawater-precipitated cherts. Finally, we identify a link between temporal variations in the O isotope composition of silicified lavas and cherts and in the O isotope variations occurring in the Barberton TTGs. It is noteworthy that we differentiate here “regional metamorphism” from “seafloor hydrothermalism”. Seafloor hydrothermal processes are near-contemporaneous with sedimentation and eruption of the studied rocks, while regional metamorphism significantly postdates these events.

4.1. Effects of regional metamorphism

The temperature of regional metamorphism in the Onverwacht Group has already been constrained to 300–450 °C by analyses of chlorite chemistry (Xie et al., 1997) and Raman spectrometry of carbonaceous materials (Tice et al., 2004). A voluminous flow of metamorphic fluids may have an effect on the measured O isotope compositions of cherts because O is abundant in most fluids. Previously,

$\delta^{18}\text{O}$ values that are lower than ~16 ‰ measured in cherts from basal formations of the Onverwacht Group (i.e. Komati and Hooggenoeg Formations) (Fig. 3) were ascribed to the circulation of regional metamorphic fluids at 300–400 °C around 3.45 Ga, and therefore discarded from Paleoenvironmental reconstructions (Knauth and Lowe, 2003). However, thermometric analyses based on chlorite composition and Raman spectrometry of carbonaceous materials identify the 300–400 °C regional metamorphic event even in the stratigraphically upper Buck Reef Chert and Mendon cherts that were argued to preserve seawater-derived elevated $\delta^{18}\text{O}$ values (Figs. 2, 5 and 6) (Alleon et al., 2021; Tice et al., 2004; Zakharov et al., 2021). Independent thermometers (e.g. chlorite compositions and Raman spectrometry of carbonaceous matter) have demonstrated that a 300–400 °C metamorphic event affected all the silicified lithologies of the Barberton Greenstone Belt regardless of their stratigraphic position (Grosch, 2018; Tice et al., 2004; Xie et al., 1997). This eliminates regional metamorphism as the primary cause of the observed isotopic differences between the lower (i.e. Middle Marker and Hooggenoeg) and upper (i.e. Buck Reef and Mendon) chert layers of the Onverwacht Group (Fig. 1b). For regional metamorphism to significantly alter the O isotope composition of cherts, it would require operating at high fluid/rock ratio (that is metamorphic fluid, not the original seawater-derived hydrothermal fluids) to recrystallize the silica with fluid isotope composition far from equilibrium, or it would need to re-homogenise the silica phases with other minerals (e.g., Hyslop et al., 2008). Re-crystallisations at relatively low fluid/rock ratio during

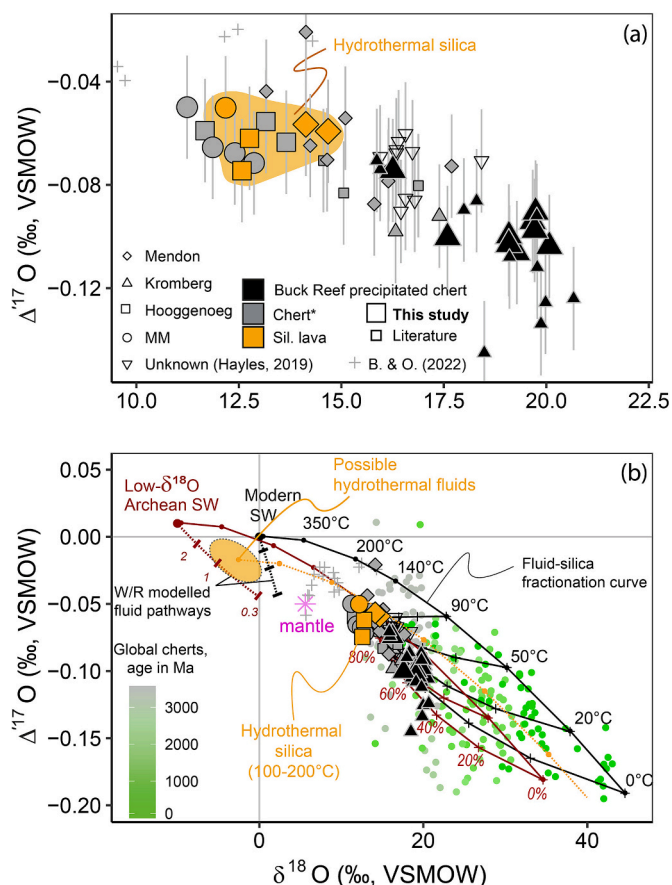


Fig. 6. Triple O isotopic compositions of the Onverwacht cherts and silicified lavas analysed in this study compared with previous analyses of the Onverwacht cherts (Hayles et al., 2019; Lowe et al., 2020; Sengupta and Pack, 2018; Zakharov, Marin-Carbonne, et al., 2021) and with the global record of cherts (Zakharov et al., 2021). For comparison, silicified lavas from the Nuvvuagittuq greenstone belt (Bindeman and O'Neil, 2022) are shown as grey crosses. The fractionation curve between silica and fluids are drawn after the equations of Sharp et al. (2016). The star (*) on cherts indicates that they comprise pervasively silicified clastic sediments that we analysed and cherts of unknown nature from the literature that may be both silicified clastic sediments and seawater-precipitated cherts. The proposed field of hydrothermal silica and fluids are shown in orange. The 'W/R modelled fluid pathways' are based on numerical models of water-rock interactions and calculations of triple O isotopic composition of the fluids at equilibrium. Results of mixing calculations between pure seawater-precipitated and hydrothermal silica are also shown considering two different compositions for the Archean seawater: one with a low $\delta^{18}\text{O}$ value of -10 ‰ and another one with a modern-day like oceanic composition ($\delta^{18}\text{O} = 0$ ‰).

regional metamorphism are unlikely to have importantly affected the isotopic composition of analysed silica (Marin-Carbonne et al., 2014; Perry and Tan, 1972). Consequently, based on consistent regional metamorphism temperature spanning the Komati to the Mendon formation, this event is unlikely to explain the difference in $\delta^{18}\text{O}$ values displayed by cherts and silicified lavas across the Onverwacht Group (Figs. 3 and 5). Thus, the O isotope composition of silica phases from silicified lavas, silicified clastic sediments and seawater-precipitated cherts provide critical insight into reconstructing the temperature and composition of Palaeoarchean hydrothermal fluids and seawater from which they precipitated.

4.2. Insights for isotopic composition of Palaeoarchean hydrothermal fluids

Geologic evidence (e.g. presence of micro-quartz veins and brecciation) demonstrated that silicified lavas and clastic sediments formed through interaction of original rocks with hydrothermal fluids (e.g. Hofmann and Harris, 2008; Paris et al., 1985). Although the O and Si isotope composition of these hydrothermal fluids remain poorly constrained, their determination may ameliorate constrains on seawater composition and temperature (e.g. Knauth and Lowe, 2003; Lowe et al., 2020; Tatzel et al., 2024). In fact, the stable isotope composition of hydrothermal fluids depends on the composition of the seawater and oceanic crust that preside over their formation, and on the thermodynamic conditions (e.g. temperature) of seawater-crust interaction (e.g. Abraham et al., 2011; Zakharov et al., 2021). Here we use the O and Si isotopic composition of the pervasively silicified lavas and cherts that we have analysed to constrain the isotopic composition of the Palaeoarchean silicifying hydrothermal fluids. The pervasive silicification of the analysed silicified clastic sediments and lavas (e.g. Figs. 2 and 4) informs that they are dominantly constituted by hydrothermal silica, and are therefore ideal for constraining hydrothermal fluids.

The average $\delta^{30}\text{Si}$ values of the silicified clastic sediments and lavas are generally positive ($> +0.19$ ‰). These values suggest that kinetic fractionations did not intervene during hydrothermal silicification as kinetic fractionation would produce negative $\delta^{30}\text{Si}$ in hydrothermal silica (Kleine et al., 2018). Although a model of dynamic fractionation of Si isotopes between fluids and precipitating silica has been used for thermometric purposes (Dupuis et al., 2015; Tatzel et al., 2024), Abraham et al. (2011) observed a gradual increase $\delta^{30}\text{Si}$ values upwards silicified lavas flows that they ascribed to a Rayleigh-type fractionation in the fluids due to silica precipitation. This complicates the use of a dynamic model to recalculate the possible Si isotopic composition of silicifying fluids. We note however that the $\delta^{30}\text{Si}$ values of the silicified clastic sediments and lavas are as positive as most seawater-precipitated cherts of Palaeoarchean age (Geilert et al., 2014; Marin-Carbonne et al., 2011; van den Boorn et al., 2007, 2010). Similarly positive $\delta^{30}\text{Si}$ values were also measured in the quartz cements of silicified lavas from the Abitibi greenstone belt (Bregman et al., 2016), suggesting that such hydrothermal silica were commonly heavy in Si isotopes during the Archean Eon. We therefore propose that the different fluids involved in the precipitation of silica near the palaeoarchean seafloor, namely the Palaeoarchean seawater and hydrothermal fluids, displayed similar Si isotope composition.

Mostly negative $\delta^{30}\text{Si}$ values were measured in the seawater-precipitated cherts and interpreted to reflect a post-depositional input of hydrothermal fluids (Geilert et al., 2014; Sun et al., 2023; Van Den Boorn et al., 2007; Van den Boorn et al., 2010). However, the positive $\delta^{30}\text{Si}$ values that we have measured in hydrothermally silicified lavas and clastic sediments rather support the alternative model that negative $\delta^{30}\text{Si}$ values of some cherts may be due to Rayleigh dynamic fractionation (Marin-Carbonne et al., 2011) or kinetic fractionation (Kleine et al., 2018). Sugitani (1992) proposed that aqueous Si content of Archean seawater was primarily derived from hydrothermal fluid discharges, and this view supported by the similarity in $\delta^{30}\text{Si}$ between seawater-precipitated cherts and hydrothermally-silicified clastic sediments and lavas.

The O isotope composition of silica fractions is consistent with hydrothermal silicification of the analysed clastic sediments and lava samples that we analysed. These samples have an O isotope composition ($\delta^{18}\text{O} = 11.3$ – 14.8 ‰ and $\Delta^{17}\text{O} = -0.05$ to -0.07 ‰) which differs from that of the seawater-precipitated Buck Reef Cherts ($\delta^{18}\text{O} = 16.4$ to 20.3 ‰ and $\Delta^{17}\text{O} = -0.07$ to -0.1 ‰) (Fig. 6). Contrary to previous suggestions (e.g. Lowe et al., 2020), even the triple O isotope composition of Buck Reef cherts is not compatible with simple precipitation from seawater (see Section 4.3.). Considering the previously proposed temperature range of hydrothermal silicification (i.e. 100–200 °C)

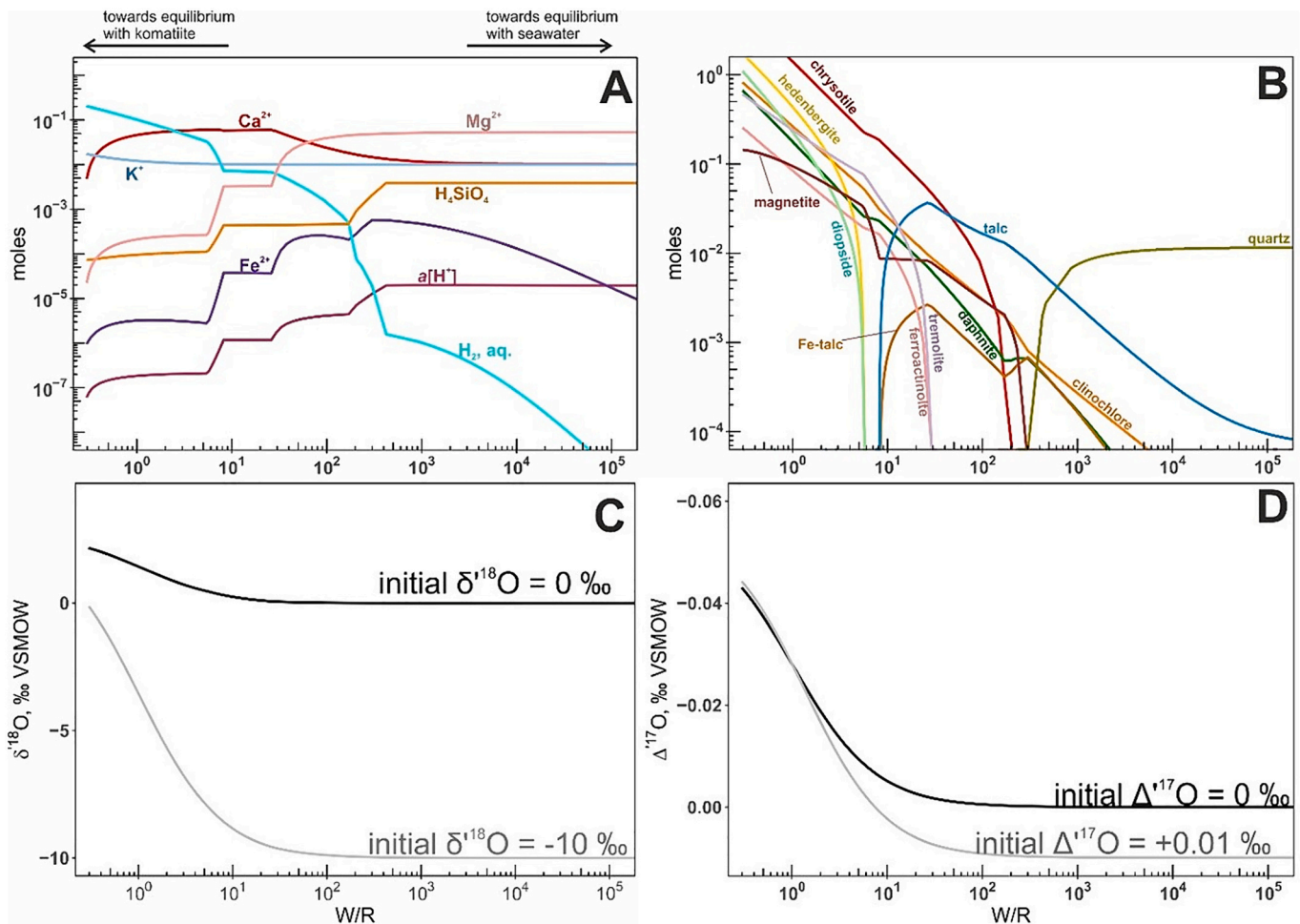


Fig. 7. Graphic representation of the output of the aqueous-mineral equilibrium modelling coupled with O isotopes. The komatiite-seawater reaction is computed in CHIM-XPT and is post-processed for O isotope calculation (see **Supplementary File A**). The horizontal axes in all panels denote the compositional change of the system due to titration progress of komatiite into the 1020 g of seawater solution. The mass ratio of titrated komatiite to solution is shown as water/rock ratio (W/R). A) Total moles of major dissolved component species that show significant variations controlled by aqueous-mineral equilibria, excluding Na^+ , Cl^- , Al^{3+} , HCO_3^- and SO_4^{2-} . In addition, a measure of pH is shown in terms of aqueous activity of H^+ species ($a[\text{H}^+]$). Molality of aqueous H_2 is also shown to emphasize the reducing nature of the reaction. A list of individual aqueous species and their molalities is given in **Supplementary File A**. B) Moles of equilibrium minerals produced by the komatiite-seawater reaction. C) The computed $\delta^{18}\text{O}$ value of the equilibrium H_2O is shown for two initial compositions – modern-day like seawater (initial $\delta^{18}\text{O} = 0$ ‰) and a potential low- $\delta^{18}\text{O}$ Archean seawater (initial $\delta^{18}\text{O} = -10$ ‰). D) The computed $\Delta^{17}\text{O}$ values of the equilibrium H_2O . Full list of equilibrium mineral-water fractionation factors is given in **Supplementary Material 3**. The theta value of 0.527 is used to calculate the triple O isotope fractionation factors $17/16\alpha = 18/16\alpha\theta$.

(Abraham et al., 2011; Cloete, 1991; de Wit and Furnes, 2016; Hofmann and Harris, 2008; Lowe and Byerly, 1986), we calculate a range of isotopic composition for hydrothermal fluids and obtain negative $\delta^{18}\text{O}$ (–8 to 0 ‰) and $\Delta^{17}\text{O}$ values (–0.04 to 0 ‰) (Fig. 6). Although silicification of lavas and clastic sediments resulted from both descending flux a seawater-derived of fluids and an ascending flux derived from the deep crust, our rough estimation cannot definitively discriminate the O isotope composition of each one of these fluids. Yet, we observe that the negative $\delta^{18}\text{O}$ values calculated for Archean hydrothermal fluids differ positive $\delta^{18}\text{O}$ values measured for modern hydrothermal fluids (Elderfield et al., 1999; Shanks, 2001; Zakharov et al., 2021a), although both fluids depict negative $\Delta^{17}\text{O}$. This could be due to a different seawater composition during the Palaeoarchean Era.

Our model of seawater-komatiite reaction (Fig. 7) can provide a first-order estimation the most likely composition of seawater that existed during the Palaeoarchean Era. In the model, hydrothermal fluids obtained using a virtual Archean seawater with an extremely low $\delta^{18}\text{O}$ of –10 ‰ and a $\Delta^{17}\text{O}$ of 0.01 ‰ (Jaffrés et al., 2007) roughly reproduces the negative $\delta^{18}\text{O}$ of hydrothermal fluids reconstructed from silica compositions (Fig. 6). This supports lower $\delta^{18}\text{O}$ value in Archean oceans

compared to modern analogues (Bindeman and O’Neil, 2022; Jaffrés et al., 2007), although it cannot allow estimating the exact $\delta^{18}\text{O}$ value of the Palaeoarchean seawater. According to the model, modern seawater-derived hydrothermal fluids is too high in $\delta^{18}\text{O}$ to explain the O isotope composition of measured silicified lavas and clastic sediments. Although Sengupta et al. (2020) proposed a high $\delta^{18}\text{O}$ of ~1 ‰ for the Archean seawater, recent numerical modelling studies are consistent with our results as they also suggested a low $\delta^{18}\text{O}$ of –2 to –10 ‰ in the Palaeoarchean seawater (Herwartz et al., 2021; Tatzel et al., 2022).

4.3. Post-depositional modification of seawater-precipitated cherts

While we provide new measurements of seawater-precipitated cherts, it has been recognized that near-seafloor diagenesis of cherts is an important factor controlling the O isotope composition of final cherts (Ibarra et al., 2022; Kolodny and Epstein, 1976; Marin-Carbonne et al., 2011; Yanchilina et al., 2020; Zakharov et al., 2023). With the novel triple O isotope data, we observe that seawater-precipitated cherts such as the Buck Reef Cherts exhibit an evolution from the hydrothermal silica endmember towards higher $\delta^{18}\text{O}$ and lower $\Delta^{17}\text{O}$ values (Fig. 6a).

The hydrothermal component is constrained here by measurements of silicified rocks produced by precipitation of silica from hydrothermal fluids (Fig. 6a) (Hofmann and Harris, 2008).

A simple mixing model of measured hydrothermal silica (i.e. silicified rocks) with estimated seawater-precipitated silica (Fig. 6b) in the triple O space reproduces the variation of O isotope composition in seawater-precipitated cherts. However, both a modern-day-like seawater displaying $\delta^{18}\text{O}$ close to 0 ‰ (Knauth and Lowe, 1978, 2003; Lowe et al., 2020) and assumed Archean seawater with an extremely low $\delta^{18}\text{O}$ of -10 ‰ (Jaffrés et al., 2007; Tatzel et al., 2022) allow the mixing model to cover the full range of seawater-precipitated chert compositions. Additionally, seawater temperatures of 0 to 60 °C are all capable of reproducing the O isotope composition of seawater-precipitated cherts from the Onverwacht Group. Thus, due to post-depositional interaction of seawater-precipitated cherts with hydrothermal fluids, it is difficult to reconstruct Archean seawater compositions or temperatures in a straightforward manner using chert's isotopic composition. Indeed, post-depositional fluid circulations at diagenetic stage create complex mixing schemes even in the triple O isotope compositions of the Cenozoic seawater-precipitated cherts recovered from the modern seafloor (see compilation in Fig. 6) (Ibarra et al., 2022; Kolodny and Epstein, 1976; Yanchilina et al., 2020).

4.4. Origin of stratigraphic variations in O isotope compositions

The $\delta^{18}\text{O}$ values of silicified lavas and cherts increase up the stratigraphic section of the Onverwacht group (Fig. 3 and 5a), unlike $\delta^{30}\text{Si}$ values that do not change considerably through the stratigraphic section. The lowermost member measured here is Middle Maker and shows $\delta^{18}\text{O}$ values of 10–13 ‰ and the uppermost member, Medon 1, has a $\delta^{18}\text{O}$ of ~ 15 ‰, that extends up to 20 ‰ if we consider previously published data (Fig. 5a). While Si isotopes do not display this evolution, the stratigraphic variation of O isotope represents an important signal recorded in the Onverwacht Group (Fig. 3) but its origin remains unconstrained (de Wit and Furnes, 2016; Knauth and Lowe, 1978, 2003).

To understand the primary causes behind the stratigraphic variations in $\delta^{18}\text{O}$ values of cherts and silicified lavas, we consider the theoretical dependence of their O isotope composition on several factors: (1) the composition of the Archean seawater, (2) the composition of the reacting crustal formations, (3) the ratio of interacting water/rock abundances, and (4) the thermal condition of the system during silica precipitation or seafloor silicification. The three first variables are unlikely to have played a major role in the case of the Onverwacht formations for the following reasons. First, it is difficult to explain a $\delta^{18}\text{O}$ variation of >4 ‰ in seawater during the 180 Ma in which the seafloor formation cropping out to the North of Komati fault emplaced (Fig. 1). Although the details of Archean O isotope mass balance are not well-constrained, the change of >4 ‰ over a course of 180 Ma is unlikely. This is due to mass-balance considerations of the O isotope budget. The residence timescale for O in seawater is large (i.e. several tens of Ma) due to its abundance reflecting relative sizes of its sources and sinks (Muehlenbachs, 1998). Specifically, buffering by the balance of seawater circulation in the greenstone formations and weathering is unlikely to change the composition of seawater in a dramatic fashion (Meuhlenbachs and Clayton, 1976). Secondly, the variability of $\delta^{18}\text{O}$ in the pre-silicified rocks is also expected to be minimal because the Komati, Hooggenoeg and Mendon lavas are all mantle-derived komatiites with $\delta^{18}\text{O}$ likely around 5.5 ± 1 ‰ (Valley et al., 1998) (Figs. 2 and 5a-c). Finally, although the fluid/rock ratio of former hydrothermal reactions is quite hard to estimate (Alt and Bach, 2006; Coogan and Gillis, 2018), all the studied samples were pervasively silicified to a similar extent (> 90 vol% quartz) supporting constant fluid/rock ratios during hydrothermal fluid circulations (Abraham et al., 2011; Duchac and Hanor, 1987; Paris et al., 1985). Based on this argumentation, the changes in thermal conditions of the hydrothermal systems (e.g. Tatzel et al., 2022) might be a critical component explaining the increase of

$\delta^{18}\text{O}$ values between 3.48 and 3.3 Ga.

We propose that the stratigraphic variations of O isotope compositions in the Onverwacht silicified lavas and cherts was due to local lithospheric cooling associated with the evolution of the Barberton Greenstone Belt. The secular and global cooling of the Earth has been demonstrated to largely explain $\delta^{18}\text{O}$ changes observed in global chert compilations (Tatzel et al., 2022). Similarly, a local lithospheric cooling related to the evolution of the Barberton Greenstone Belt would account for the upward increase of $\delta^{18}\text{O}$. As the silicification of seafloor lava and the formation of overlying chert layers occurred likely on a timescale exceeding 1 Ma, volcanic eruptions are not considered to be the main driver of heat during the hydrothermal circulations. Regional geothermal gradient is a possible candidate as the source of heat for hydrothermal circulation of seawater-derived hydrothermal fluids that caused silicification. The evolution of the Barberton Greenstone Belt from a hot, thin and juvenile greenstone succession to a relatively colder, thicker and stable continent (Drabon et al., 2019, 2024; Lowe and Byerly, 2007) might have been accompanied by a progressive cooling at lithospheric scale that explains the long-term and vertical increase of $\delta^{18}\text{O}$ values in cherts and silicified lavas of the Onverwacht Group.

4.5. Implications for the origin of Archean granitoids

Although there is no physical relationship between the analysed silica-rich rocks and granitoids of the Barberton area, the evolution of O and Si isotopic compositions in these rocks offers insights into the composition of analogous lithologies reworked in the source zone of the Barberton TTGs (André et al., 2022). Elevated $\delta^{18}\text{O}$ (4.4–6.9 ‰, measured in zircon) and $\delta^{30}\text{Si}$ values (-0.14 to 0.25 ‰: measured whole rock and zircon composition) were recently published for the Barberton granitoids (Fig. 8). These data were interpreted to support the reworking of seafloor-derived silicified lavas and cherts in the source zone of the Barberton granitoids (André et al., 2019; Deng et al., 2019; Lei et al., 2023; Wang et al., 2022). Notably, similar Si but different O isotope compositions have been observed between the pre-3.3 Ga ($\delta^{18}\text{O} = 4.4$ –6.0 ‰ and $\delta^{30}\text{Si} = -0.05$ to 0.20 ‰) and post-3.3 Ga granitoids ($\delta^{18}\text{O} = 4.9$ –6.9 ‰ and $\delta^{30}\text{Si} = -0.14$ to 0.17 ‰) (Fig. 8). To explain this decoupled evolution of O and Si isotopes in the granitoids, we propose that it reflects the near-constant $\delta^{30}\text{Si}$ values and chronostratigraphically increasing $\delta^{18}\text{O}$ values (from 10 to 12 ‰ to 16–19 ‰) of silicified clastic sediments and lavas derived from the seafloor (Figs. 3, 5 and 7). In this perspective, the older seafloor-derived silica that was reworked into 3.45 Ga TTGs was likely lower in $\delta^{18}\text{O}$ than the younger seafloor-derived silica reworked in post-3.3 Ga TTGs, but they all must have displayed a similar range of $\delta^{30}\text{Si}$ values. If true, then an increasing fraction of younger seafloor-derived components was incorporated in the source zone of younger granitoids. This demonstrates a close link between mafic rocks emplaced at the surface of the Earth and their recycling into the source zone of Palaeoarchean granitoids. Determining the exact age of the silicified rocks that were reworked in the source zone of the Barberton TTGs remains challenging, but previous Nd and Hf isotopic measurements in the TTGs suggested that their source was still juvenile upon melting (Moyen et al., 2019). Thus, the Onverwacht rocks might be very close in composition to seafloor-derived lithologies reworked in the source zone of the Barberton granitoids. Unlike other terrains where TTG melts have been proposed to originate from the same Hadean crust over more than 1 Ga based on ^{146}Nd – ^{142}Nd isotope analyses (e.g. O'Neil and Carlson, 2017), we suggest that different generations of seafloor-derived components were systematically recycled into the source zone of the Barberton granitoids over time. Thus, various mechanisms for forming granitic rocks may have co-existed on the primitive Earth.

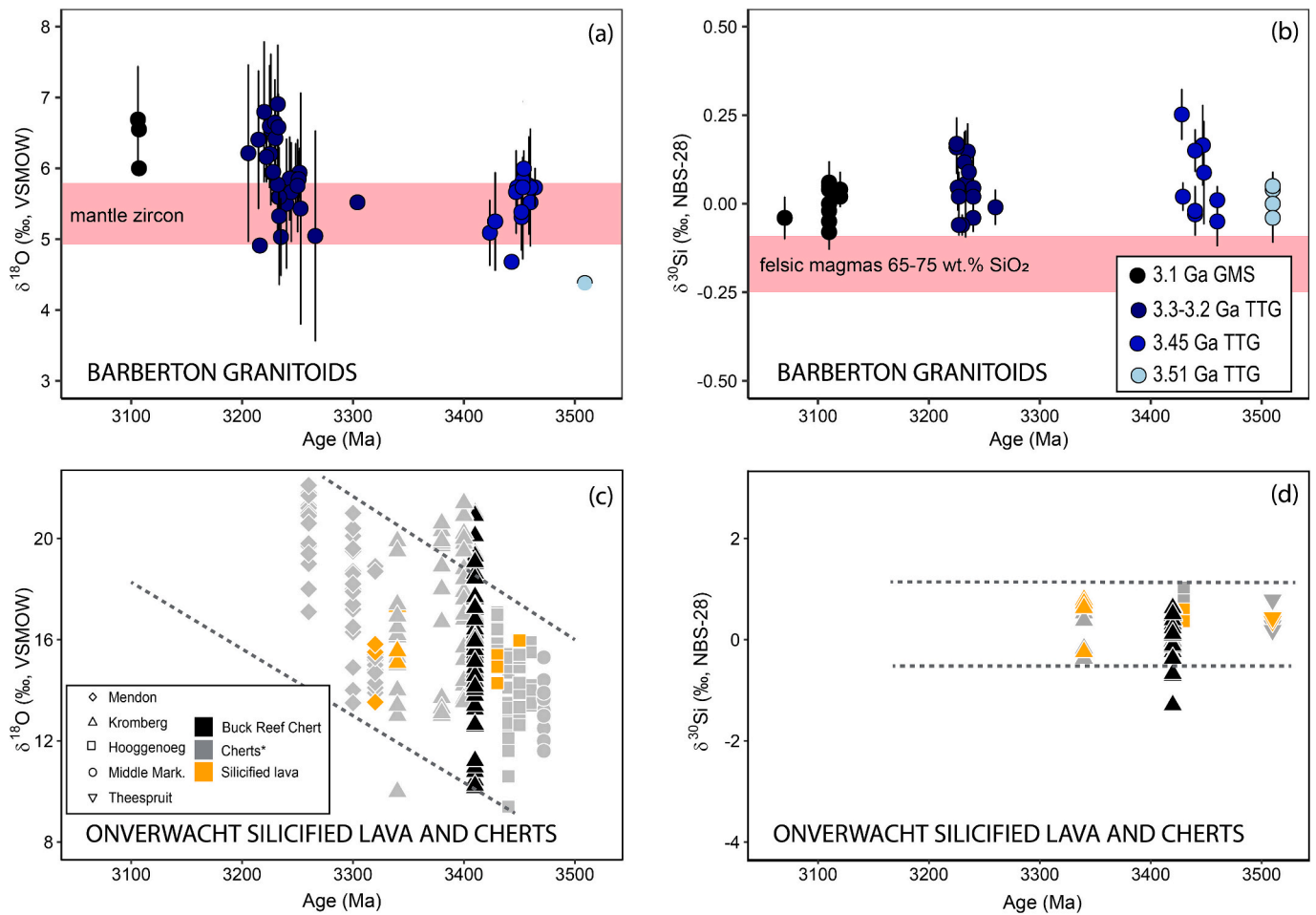


Fig. 8. Variations of $\delta^{18}\text{O}$ in zircons (a) and $\delta^{30}\text{Si}$ in TTG magmas (b) in the Barberton granitoids compared with the evolution of $\delta^{18}\text{O}$ (c) and $\delta^{30}\text{Si}$ (d) in the Onverwacht silicified lava and cherts. Compositions featured in plates (a) and (b) were compiled from previously published datasets (André et al., 2019; Deng et al., 2019; Lei, Wang, et al., 2023; Valley et al., 2005; Wang et al., 2022). Oxygen isotopic compositions were exclusively measured from magmatic zircons whereas silicon isotopic ratios include measurements from the bulk-rock but also from zircons. The equation of Guitreau et al. (2022) was used to convert the $\delta^{30}\text{Si}$ values of zircons into the magmatic values shown on the Figure. Note that $\delta^{30}\text{Si}$ signatures are higher than mantle values in all the Barberton TTGs, whereas $\delta^{18}\text{O}$ signatures only reach notably elevated only in those that are younger than 3.23 Ga. The symbols of (c) and (d) are the same as in Figs. 3 and 6. The star (*) on cherts in the legend indicates that they may comprise pervasively silicified clastic sediments and seawater-precipitated cherts that were not clearly distinguished in the literature.

5. Conclusion

- The compositions of silicified clastic sediments and lava, and seawater-precipitated cherts of the Onverwacht Group, Barberton Greenstone Belt constrain the hydrothermal silica endmember in the triple O isotope space. The silicified rocks have lower $\delta^{18}\text{O}$ (silicified lava = 12.3–14.9‰ and silicified clastic sediments = 11.3–14.2‰) and higher $\Delta^{17}\text{O}$ values (−0.07 to −0.05‰) than seawater-precipitated cherts (16.4 to 20.3‰ of $\delta^{18}\text{O}$ and −0.12 to −0.07‰ of $\Delta^{17}\text{O}$). These values are best explained by low-temperature (100–200 °C) hydrothermal alteration that obscure the record of seawater temperature and composition in pure seawater-precipitated cherts.
- Considering the possible silicification temperature range of 100–200 °C, the triple O isotope composition of Archean silicifying fluid is likely negative in both $\delta^{18}\text{O}$ and $\Delta^{17}\text{O}$. Numerical modelling of komatiite-seawater reaction and mass-balance calculation of O isotope composition in equilibrium fluids suggest that the silicifying hydrothermal fluids must have originated from a Palaeoarchean seawater with a negative $\delta^{18}\text{O}$ value. However, the exact O isotope composition and temperature of this Palaeoarchean seawater is challenging to reconstruct.

- A slight but evident increase of $\delta^{18}\text{O}$ values upwards the Onverwacht stratigraphy (from ~10–13‰ to 15–20‰) is observed both in the hydrothermally silicified lavas and clastic sediments. As changes in seawater $\delta^{18}\text{O}$ and temperature are unlikely to evolve dramatically over the formation of the Onverwacht Group, this variation is likely due to lithospheric cooling of the Barberton Greenstone Belt over time.
- The exclusively positive values of average $\delta^{30}\text{Si}$ (+0.19 to +1.24‰) measured in the hydrothermally silicified lava are like positive $\delta^{30}\text{Si}$ values that were previously ascribed to Archean seawater-precipitated cherts, suggesting that seawater-derived and hydrothermal silica were relatively close in Si isotopic composition.
- The evolution of $\delta^{18}\text{O}$ and $\delta^{30}\text{Si}$ values observed in silicified rocks from the Onverwacht Group is correlated with evolutions observed in the Barberton granitoids over time, suggesting that different generations of granitoid sources reworked distinct generations of seawater-derived rocks. Accordingly, at least in some parts of the Palaeoarchean Earth, the recycling of seafloor-derived rocks into the deep source of granitoids might have been active. This insight enhances our understanding of the geological processes that contributed to the formation of ancient granitic complexes.

Supplementary data to this article can be found online at <https://doi.org/10.1016/j.chemgeo.2024.122407>.

org/10.1016/j.chemgeo.2024.122407.

CRedit authorship contribution statement

L.S. Kitoga: Writing – review & editing, Writing – original draft, Visualization, Methodology, Investigation, Formal analysis, Data curation, Conceptualization. **D. Zakharov:** Writing – review & editing, Validation, Investigation, Formal analysis. **J. Marin-Carbonne:** Writing – review & editing, Validation, Supervision, Funding acquisition, Formal analysis, Conceptualization. **M. Boyet:** Writing – review & editing, Validation, Conceptualization. **J.-F. Moyen:** Writing – review & editing, Funding acquisition, Conceptualization. **T. Di Rocco:** Writing – review & editing, Formal analysis. **A. Pack:** Writing – review & editing, Formal analysis. **N. Olivier:** Writing – review & editing, Validation, Data curation. **G. Stevens:** Writing – review & editing, Resources.

Declaration of competing interest

The authors declare that they have no known competing financial interests or personal relationships that could have appeared to influence the work reported in this paper.

Data availability

All the data is submitted along with the manuscript and supplementary files.

Acknowledgements

The results presented here are part of the PhD research of L.S. Kitoga funded by the French Centre National de la Recherche Scientifique. This study was financially supported by the BUCOMO collaborative project of J-F Moyen (UCA) and G. Stevens (Stellenbosch University), the European Research council (ERC) under the European Union's Horizon H2020 research and innovation program (STROMATA grant agreement 759289, ISOREE grant agreement 682778), and a CAP 20-25 travel grant to Switzerland awarded by UCA to L.S. Kitoga. The authors sincerely acknowledge the assistance of Anne-Sophie Bouvier, Jean-Luc Devidal, Thomas Bovay, Julien Alléon and Geeth Manthilake, Torsten Vennemann during sample preparations and analytical sessions. A. Hofmann is thanked for provision of the IODP Buck Reef samples and Martin Guitreau for valuable discussions on O and Si isotopic compositions of Archean granitoids. This is Laboratory of Excellence ClerVolc contribution n°XX.

References

- Abraham, K., Hofmann, A., Foley, S.F., Cardinal, D., Harris, C., Barth, M.G., Andre, L., 2011. Coupled silicon-oxygen isotope fractionation traces Archean silicification. *Earth Planet. Sci. Lett.* 301 (1–2), 222–230.
- Alleon, J., Bernard, S., Olivier, N., Thomazo, C., Marin-Carbonne, J., 2021. Inherited geochemical diversity of 3.4 Ga organic films from the Buck Reef Chert, South Africa. *Communications Earth and Environment* 2 (1), 4–10.
- Alt, J.C., Bach, W., 2006. Oxygen isotope composition of a section of lower oceanic crust, ODP Hole 735B. *Geochem. Geophys. Geosyst.* 7 (12).
- Alt, J.C., Laverne, C., Coggon, R.M., Teagle, D.A.H., Banerjee, N.R., Morgan, S., Smith-Duque, C.E., Harris, M., Galli, L., 2010. Subsurface structure of a submarine hydrothermal system in ocean crust formed at the East Pacific rise, ODP/IODP Site 1256. *Geochem. Geophys. Geosyst.* 11 (10), 1–28.
- André, L., Abraham, K., Hofmann, A., Monin, L., Kleinhanns, I.C., Foley, S., 2019. Early continental crust generated by reworking of basalts variably silicified by seawater. *Nat. Geosci.* 12, 769–773.
- André, L., Monin, L., Hofmann, A., 2022. The origin of early continental crust: New clues from coupling Ge/Si ratios with silicon isotopes. *Earth Planet. Sci. Lett.* 582.
- Berner, E.K., Berner, R.A., 1996. *Global Environment: Water, Air, and Geochemical Cycles*. Prentice-Hall, Englewood Cliffs, New Jersey.
- Brengman, L.A., Fedo, C.M., Whitehouse, M.J., 2016. Micro-scale silicon isotope heterogeneity observed in hydrothermal quartz precipitates from the >3.7 Ga Isua Greenstone Belt, SW Greenland. *Terra Nova* 28 (1), 70–75.
- Byerly, G.R., Kröner, A., Lowe, D.R., Todt, W., Walsh, M.M., 1996. Prolonged magmatism and time constraints for sediment deposition in the early Archean Barberton greenstone belt: evidence from the Upper Onverwacht and Fig tree groups. *Precambrian Res.* 78 (1–3 SPEC. ISS), 125–138.
- Byerly, G.R., Lowe, D.R., Heubeck, C., 2019. Geologic Evolution of the Barberton Greenstone Belt—A Unique Record of Crustal Development, Surface Processes, and early Life 3.55–3.20 Ga. In: *Earth's Oldest Rocks*. Elsevier B.V.
- Cammack, J.N., Spicuzza, M.J., Cavosie, A.J., Van Kranendonk, M.J., Hickman, A.H., Kozdon, R., Orland, I.J., Kitajima, K., Valley, J.W., 2018. SIMS microanalysis of the Strelley Pool Formation cherts and the implications for the secular-temporal oxygen-isotope trend of cherts. *Precambrian Res.* 304, 125–139.
- Cloete, M., 1991. An overview of metamorphism of the Barberton Greenstone belt. In *ICDP Project 280-two Cratons and an Orogenic Excursion Guidebook and Review Articles for a Field Workshop through selected Archean Terranes of Swaziland, South Africa and Zimbabwe*. (pp. 84–98).
- Coogan, L.A., Gillis, K.M., 2018. Low-Temperature Alteration of the Seafloor: Impacts on Ocean Chemistry. *Annu. Rev. Earth Planet. Sci.* 46, 21–45.
- de Wit, M.J., Furnes, H., 2016. 3.5-Ga hydrothermal fields and diamicrites in the Barberton Greenstone Belt-Paleoarchean crust in cold environments. *Science Advances* 2 (2), 1–12.
- de Wit, M.J., Furnes, H., Robins, B., 2011. Geology and tectonostratigraphy of the Onverwacht Suite, Barberton Greenstone Belt, South Africa. *Precambrian Res.* 186 (October 2015), 1–27.
- Deng, Z., Chaussidon, M., Guitreau, M., Puchtel, I.S., Dauphas, N., 2019. An oceanic subduction origin for Archean granitoids revealed by silicon isotopes. *Nat. Geosci.* 12 (September), 774–779.
- Drabon, N., Galic, A., Mason, P.R.D., Lowe, D.R., 2019. Provenance and tectonic implications of the 3.28–3.23 Ga Fig tree Group, Central Barberton greenstone belt, South Africa. *Precambrian Res.* 325 (July 2018), 1–19.
- Duchac, K.C., Hanor, J.S., 1987. Origin and timing of the metasomatic silicification of an early Archean komatiite sequence, Barberton Mountain Land, South Africa. *Precambrian Res.* 37, 125–146.
- Dupuis, R., Benoit, M., Nardin, E., Méheut, M., 2015. Chemical geology. Fractionation of Silicon Isotopes in Liquids: The Importance of Configurational Disorder 396 (239), 254. <https://doi.org/10.1126/science.ns-3.50.59>.
- Elderfield, H., Wheat, C.G., Mottl, M.J., Monnin, C., Spiro, B., 1999. Fluid and geochemical transport through oceanic crust: a transect across the eastern flank of the Juan de Fuca Ridge. *Earth Planet. Sci. Lett.* 172 (1–2), 151–165.
- Foley, S.F., Buhre, S., Jacob, D.E., 2003. Evolution of the Archean crust by delamination and shallow subduction. *Nature* 421 (6920), 249–252.
- Geilert, S., Vroon, P.Z., van Bergen, M.J., 2014. Silicon isotopes and trace elements in chert record early Archean basin evolution. *Chem. Geol.* 386, 133–142.
- Grosch, E.G., 2018. *Metamorphic Processes Preserved in Early Archean Supracrustal Rocks of the Barberton Greenstone Belt*. Geological Society Special Publication, South Africa, p. 478.
- Grosch, E.G., Slama, J., 2017. Evidence for 3.3-billion-year-old oceanic crust in the Barberton greenstone belt, South Africa. *Geology* 45 (8), 695–698.
- Guitreau, M., Gannoun, A., Deng, Z., Chaussidon, M., Moynier, F., Barbarin, B., Marin-Carbonne, J., 2022. Stable isotope geochemistry of silicon in granitoid zircon. *Geochim. Cosmochim. Acta* 316, 273–294.
- Hanor, J.S., Duschac, K.C., 1990. Isovolumetric Silicification of early Archean Komatiites: Geochemical Mass Balances and Constraints on Origin. *J. Geol.* 98 (6), 863–877.
- Hayles, J.A., Yeung, L.Y., Homann, M., Banerjee, A., Jiang, H., Shen, B., Lee, C.-T., 2019. Three billion Year Secular Evolution of the Triple Oxygen Isotope Composition of Marine Chert. *Earth Planet. Sci. Lett.* 1–30.
- Herwartz, D., Pack, A., Nagel, T.J., 2021. A CO₂ greenhouse efficiently warmed the early Earth and decreased seawater 18O/16O before the onset of plate tectonics. *Proc. Natl. Acad. Sci.* 118, 1–5.
- Hofmann, A., 2005. The geochemistry of sedimentary rocks from the Fig Tree Group, Barberton greenstone belt: Implications for tectonic, hydrothermal and surface processes during mid-Archean times. *Precambrian Res.* 143, 23–49.
- Hofmann, A., Harris, C., 2008. Silica alteration zones in the Barberton greenstone belt: a window into subsurface processes 3.5–3.3 Ga ago. *Chem. Geol.* 257, 224–242.
- Hofmann, A., Bolhar, R., Orberger, B., Foucher, F., 2013. Cherts of the Barberton Greenstone Belt, South Africa: Petrology and Trace-Element Geochemistry of 3.5 to 3.3 Ga Old Silicified Volcaniclastic Sediments. *S. Afr. J. Geol.* 116 (2), 297–322.
- Hofmann, A., Jodder, J., Xie, H., Bolhar, R., Whitehouse, M., Elburg, M., 2022. The Archean geological history of the Singhbhum Craton, India – a proposal for a consistent framework of craton evolution. *Earth Sci. Rev.* 228 (January), 103994.
- Holmden, C., Muehlenbachs, K., 1993. The 18O/16O Ratio of 2-Billion-Year-Old Seawater Inferred from Ancient Oceanic Crust. *Science* 259, 1733–1736.
- Hyslop, E.V., Valley, J.W., Johnson, C.M., Beard, B.L., 2008. The effects of metamorphism on O and Fe isotope compositions in the Biwabik Iron Formation, northern Minnesota. *Contrib. Mineral. Petrol.* 155(3), 313–328.
- Ibarra, D.E., Yanchilina, A.G., Lloyd, M.K., Methner, K.A., Chamberlain, C.P., Yam, R., Shemesh, A., Stolper, D.A., 2022. Triple oxygen isotope systematic of diagenetic recrystallization of diatom opal-a to opal-CT to microquartz in deep sea sediments. *Geochim. Cosmochim. Acta* 320, 304–323.
- Jaffrés, J. B. D., Shields, G. A., Wallmann, K., 2007. The oxygen isotope evolution of seawater: a critical review of a long-standing controversy and an improved geological water cycle model for the past 3.4 billion years. *Earth Sci. Rev.* 83(1–2), 83–122.
- Kleine, B.I., Stefánsson, A., Halldórsson, S.A., Whitehouse, M.J., Jónasson, K., 2018. Silicon and oxygen isotopes unravel quartz formation processes in the Icelandic crust. *Geochemical Perspectives Letters* 7, 5–11.
- Knauth, L.P., Lowe, D.R., 1978. Oxygen isotope geochemistry of cherts from the Onverwacht (3.4 billion years) Group, Transvaal, South Africa, with implications for

- secular variations in the isotopic composition of cherts. In *Earth and Planetary Science Letters* 41.
- Knauth, L.P., Lowe, D.R., 2003. High Archean climatic temperature inferred from oxygen isotope geochemistry of cherts in the 3.5 Ga Swaziland Supergroup, South Africa. *Geol. Soc. Am. Bull.* 5, 566–580.
- Kolodny, Y., Epstein, S., 1976. Stable isotope geochemistry of deep sea cherts. *Geochim. Cosmochim. Acta* 40 (10), 1195–1209.
- Lanier, W.P., Lowe, D.R., 1982. Sedimentology of the middleker (3.4 Ga), Onverwacht group, Transvaal, South Africa. *Precambrian Res.* 18, 237–260.
- Ledevin, M., Arndt, N., Simionovici, A., Jaillard, E., Ulrich, M., 2014. Silica precipitation triggered by clastic sedimentation in the Archean: New petrographic evidence from cherts of the Kromberg type section, South Africa. *Precambrian Res.* 255, 316–334.
- Ledevin, M., Arndt, N., Chauvel, C., Jaillard, E., Simionovici, A., 2019. The sedimentary origin of black and white banded cherts of the Buck Reef, Barberton South Africa. *Geosciences (Switzerland)* 9 (10), 17–24.
- Lei, K., Wang, H., Wang, X., Zhang, Q., Li, X., 2023. Decoupled Zircon Si–O isotopes Tracing the Supracrustal Silicification and Komatiitic-Derived Fluids in the source of TTGs. *Geophys. Res. Lett.* 50 (16), 1–9.
- Lowe, D.R., Byerly, G.R., 1986. Archean flow-top alteration zones formed initially in a low-temperature sulphate-rich environment. *Nature* 324, 245–248.
- Lowe, D.R., Byerly, G.R., 2007. An overview of the geology of the Barberton greenstone belt and vicinity: Implications for early crustal development. In: Van Kranendonk, M. J., Smithies, R.H., Bennett, V.C. (Eds.), *Developments in Precambrian Geology*, Vol. 15, Issue 07. Elsevier B.V., pp. 481–526.
- Lowe, D.R., Ibarra, D.E., Drabon, N., Chamberlain, C.P., 2020. Constraints on surface temperature 3.4 billion years ago based on Triple Oxygen isotopes from the Barberton greenstone belt, South Africa, and the problem of sample selection. *Am. J. Sci.* 320 (9).
- Marin, J., Chaussidon, M., Robert, F., 2010. Microscale oxygen isotope variations in 1.9 Ga Gunflint cherts: Assessments of diagenesis effects and implications for oceanic paleotemperature reconstructions. *Geochim. Cosmochim. Acta* 74 (1), 116–130.
- Marin-Carbonne, J., Chaussidon, M., Boiron, M.-C., Robert, F., 2011. A combined in situ oxygen, silicon isotopic and fluid inclusion study of a chert sample from Onverwacht Group (3.35 Ga, South Africa): New constraints on fluid circulation. *Chem. Geol.* 286 (3–4), 59–71.
- Marin-Carbonne, J., Chaussidon, M., Robert, F., 2012. Micrometer-scale chemical and isotopic criteria (O and Si) on the origin and history of Precambrian cherts: Implications for paleo-temperature reconstructions. *Geochim. Cosmochim. Acta* 92, 129–147.
- Marin-Carbonne, J., Faure, F., Chaussidon, M., Jacob, D., Robert, F., 2013. A petrographic and isotopic criterion of the state of preservation of Precambrian cherts based on the characterization of the quartz veins. *Precambrian Res.* 231, 290–300.
- Martin, H., Moyen, J.F., Guitreau, M., Blichert-Toft, J., Le Pennec, J.L., 2014. Why Archean TTG cannot be generated by MORB melting in subduction zones. *Lithos* 198–199 (1), 1–13.
- Meuhlenbachs, K., Clayton, R.N., 1976. Oxygen Isotope Composition of the Oceanic Crust and its Bearing on Seawater. *J. Geophys. Res.* 81 (23), 4365–4369.
- O’Neil, J., Carlson, R.W., 2017. Building Archean cratons from Hadean mafic crust. *Sci. Rep.* 355 (6330), 1199–1202.
- Pack, A., Tanaka, R., Hering, M., Sengupta, S., Peters, S., Nakamura, E., 2016. The Oxygen Isotope Composition of San Carlos Olivine on the VSMOW2-SLAP2 Scale. *Rapid Communications in Mass Spectrometry*, pp. 1495–1504. April.
- Paris, I., Stanistreet, I.G., Hughes, M.J., 1985. Cherts of the Barberton greenstone belt interpreted as products of submarine exhalative activity. *J. Geol.* 93, 111–129.
- Perry, E.C., Tan, F.C., 1972. Significance of Oxygen and Carbon Isotope Variations in early Precambrian Cherts and Carbonate Rocks of Southern Africa. *Geol. Soc. Am. Bull.* 83, 647–664.
- Reed, M.H., Spycher, N.F., Palandri, J., 2010. Users Guide for CHIM-XPT: a program for Computing Reaction Processes in Aqueous-Mineral-Gas Systems and MINTAB Guide. *J. Chem. Inf. Model.* 53 (9), 1689–1699.
- Robert, F., Chaussidon, M., 2006. A paleotemperature curve for the Precambrian oceans based on silicon isotopes in cherts. *Nature* 443, 969–972.
- Rouchon, V., Orberger, B., 2008. Origin and mechanisms of K-Si-metasomatism of ca. 3.4–3.3 Ga volcanoclastic deposits and implications for Archean seawater evolution: examples from cherts of Kittys Gap (Pilbara craton, Australia) and Msauli (Barberton Greenstone Belt, South Africa). *Precambrian Res.* 165 (3–4), 169–189.
- Seitz, S., Baumgartner, L.P., Bouvier, A.S., Putlitz, B., Vennemann, T., 2017. Quartz Reference Materials for Oxygen Isotope Analysis by SIMS. *Geostand. Geoanal. Res.* 41 (1), 69–75.
- Sengupta, S., Pack, A., 2018. Triple oxygen isotope mass balance for the Earth’s oceans with application to Archean cherts. *Chem. Geol.* 495 (July), 18–26.
- Sengupta, S., Peters, S.T.M., Reitner, J., Duda, J.P., Pack, A., 2020. Triple oxygen isotopes of cherts through time. *Chem. Geol.* 554 (July), 119789.
- Shanks, W.C., 2001. Stable isotopes in seafloor hydrothermal systems: Vent fluids, hydrothermal deposits, hydrothermal alteration, and microbial processes. *Stable Isotope Geochemistry* 43, 469–525.
- Sharp, Z.D., Gibbons, J.A., Maltsev, O., Audouire, V., Pack, A., Sengupta, S., Shock, E.L., Knauth, L.P., 2016. A calibration of the triple oxygen isotope fractionation in the SiO₂-H₂O system and applications to natural samples. *Geochim. Cosmochim. Acta* 186, 105–119.
- Stefurak, E.J.T., Fischer, W.W., Lowe, D.R., 2015. Texture-specific Si isotope variations in Barberton Greenstone Belt cherts record low temperature fractionations in early Archean seawater. *Geochim. Cosmochim. Acta* 150, 26–52.
- Sugitani, K., 1992. Geochemical characteristics of Archean cherts and other sedimentary rocks in the Pilbara Block, Western Australia: evidence for Archean seawater enriched in hydrothermally-derived iron and silica. *Precambrian Res.* 57 (1–2), 21–47.
- Sun, H., Chaussidon, M., Robert, F., Tian, S., Deng, Z., Moynier, F., 2023. Triple silicon isotope insights into the formation of Precambrian cherts. *Earth Planet. Sci. Lett.* 607.
- Tamblyn, R., Hermann, J., Hasterok, D., Sossi, P., Pettko, T., Chatterjee, S., 2023. Hydrated komatiites as a source of water for TTG formation in the Archean. *Earth Planet. Sci. Lett.* 603, 117982.
- Tatzel, M., Frings, P.J., Oelze, M., Herwartz, D., Lünsdorf, N.K., Wiedenbeck, M., 2022. Chert oxygen isotope ratios are driven by Earth’s thermal evolution. *Proc. Natl. Acad. Sci.* 120, 2017.
- Tatzel, M., Oelze, M., Frick, D.A., Di Rocco, T., Liesegang, M., Stuff, M., Wiedenbeck, M., 2024. Silicon and oxygen isotope fractionation in a silicified carbonate rock. *Chem. Geol.* 658, 122120. <https://doi.org/10.1016/j.chemgeo.2024.122120>.
- Tice, M.M., Bostick, B.C., Lowe, D.R., 2004. Thermal history of the 3.5–3.2 Ga Onverwacht and Fig tree groups, Barberton greenstone belt, South Africa, inferred by Raman microspectroscopy of carbonaceous material. *Geology* 32 (1), 37.
- Valley, J.W., Kinny, P.D., Schulze, D.J., Spicuzza, M.J., 1998. Zircon megacrysts from kimberlite: Oxygen isotope variability among mantle melts. *Contrib. Mineral. Petrol.* 133 (1–2), 1–11.
- Van Den Boorn, S.H.J.M., van Bergen, M.J., Nijman, W., Vroon, P.Z., 2007. Dual role of seawater and hydrothermal fluids in early Archean chert formation: evidence from silicon isotopes. *Geology* 35 (10), 939–942.
- Van den Boorn, S.H.J.M., van Bergen, M.J., Vroon, P.Z., de Vries, S.T., Nijman, W., 2010. Silicon isotope and trace element constraints on the origin of ~3.5 Ga cherts: Implications for early Archean marine environments. *Geochim. Cosmochim. Acta* 74 (3), 1077–1103.
- Vezein, A., Pearson, D.G., Thomassot, E., Stern, R.A., Sarkar, C., Luo, Y., Fisher, C.M., 2018. Hydrothermally-altered mafic crust as source for early Earth TTG: Pb/Hf/O-isotope and trace element evidence in zircon from TTG of the Eoarchean Saglek Block, N. Labrador. *Earth and Planetary Science Letters* 503, 95–107.
- Wang, X., Tang, M., Moyen, J., Wang, D., Kröner, A., Xia, X., Xie, H., Anhaeusser, C., Hofmann, A., Li, J., Li, L., 2022. The onset of deep recycling of supracrustal materials at the Paleo-Mesoarchean boundary. *Natl. Sci. Rev.* 9, 1–9.
- Wostbrock, J.A.G., Sharp, Z.D., 2021. Triple oxygen isotopes in silica-water and carbonate-water systems. *Triple Oxygen Isotope Geochemistry* 86, 367–400.
- Xie, X., Byerly, G.R., Ferrell, R.E., 1997. Ilb trioctahedral chlorite from the Barberton greenstone belt: Crystal structure and rock composition constraints with implications to geothermometry. *Contrib. Mineral. Petrol.* 126 (3), 275–291.
- Yanchilina, A.G., Yam, R., Kolodny, Y., Shemesh, A., 2020. From diatom opal- $\delta^{18}\text{O}$ to chert $\delta^{18}\text{O}$ in deep sea sediments. *Geochim. Cosmochim. Acta* 268, 368–382.
- Yapp, C.J., 1990. Oxygen isotopes in iron (III) oxides. 1. Mineral-water fractionation factors. *Chem. Geol.* 85 (3–4), 329–335.
- Yu, H.M., Yang, L., Zhang, G.L., Huang, F., 2023. Silicon isotopic compositions of altered Oceanic crust samples from IODP U1365 and U1368: effect of low-temperature seawater alteration. *Chem. Geol.* 624 (November 2022), 121424.
- Zakharov, D.O., Marin-Carbonne, J., Alleon, J., Bindeman, I.N., 2021a. Triple Oxygen Isotope Trend Recorded by Precambrian Cherts: a Perspective from combined Bulk and in situ secondary Ion Probe Measurements. *Rev. Mineral. Geochem.* 86, 323–365.
- Zakharov, D.O., Tanaka, R., Butterfield, D.A., Nakamura, E., 2021b. A New Insight into Seawater-Basalt Exchange Reactions based on combined $\delta^{18}\text{O}$ – $\Delta^{17}\text{O}$ – $87\text{Sr}/86\text{Sr}$ Values of Hydrothermal Fluids from the Axial Seamount Volcano. *Pacific Ocean. Frontiers in Earth Science* 9 (September), 1–17.
- Zakharov, D.O., Marin-Carbonne, J., Pack, A., Di Rocco, T., Robyr, M., Vennemann, T., 2023. In-Situ and Triple Oxygen Isotope Characterization of Seafloor Drilled Cherts: Marine Diagenesis and its Bearing on Seawater Reconstructions. *Geochemistry, Geophysics, Geosystems*.
- Zheng, Y.-F., 1993. Calculation of oxygen isotope fractionation in hydroxyl-bearing silicates. *Earth Planet. Sci. Lett.* 121, 247–263.